Tectonophysics 843 (2022) 229601

Contents lists available at ScienceDirect

Tectonophysics

journal homepage: www.elsevier.com/locate/tecto

Orogenic reworking and reactivation in Central Iberia: A record of Variscan, Permian and Alpine tectonics

Diana Moreno-Martín [a,*], Rubén Díez Fernández [b], Gerardo de Vicente [c,d], Carlos Fernández [c], Juan Gómez Barreiro [e]

[a] Departamento de Mineralogía y Petrología, Universidad Complutense, 28040 Madrid, Spain
[b] Instituto Geológico y Minero de España, CSIC, 37001 Salamanca, Spain
[c] Departamento de Geodinámica, Estratigrafía y Paleontología, Universidad Complutense, 28040 Madrid, Spain
[d] Instituto de Geociencias, IGEO, CSIC-UCM, 28040 Madrid, Spain
[e] Departamento de Geología, Universidad de Salamanca, 37008 Salamanca, Spain

ARTICLE INFO

Keywords:
Extensional collapse
Tectonic inversion
Collisional orogen
Intraplate orogen
Iberian Massif

ABSTRACT

Interference between orogenic systems and deformation phases within them may lead to reworking and reactivation of previous structures. The eastern sector of the Spanish-Portuguese Central System holds evidence of two orogenic systems, Variscan and Alpine, plus a stage of Permian extension. We perform an integrated structural analysis to identify reworking and reactivation processes throughout the geological record. The Variscan record starts with crustal thickening (D_1; *E*-verging overturned folds). A second phase features the intra-orogenic collapse of an overthickened crust (D_2; top-to-the-SE ductile extensional shear zone), which produced intense structural reworking at the core of the shear zone and moderate reworking at its hanging wall. During subsequent strike-slip tectonics, crustal thickening parted transpressional deformation into a dextral shear zone and upright folds (D_3). Variscan deformation did not reactivate previous structures, but exploited a weak rheological boundary defined by contrasted lithologies (sedimentary versus igneous rocks) to accommodate D_2 shearing. Reactivation played a role afterwards: Variscan strike-slip shear zone acted as a transfer fault to accommodate Permian extension (post-orogenic collapse), and then Alpine contraction. The Permian extension record is blurred by Alpine inversion, although the trend of Alpine structures in Central Iberia, and the Spanish-Portuguese Central System, may result from Permian structural inheritance.

1. Introduction

Stress over existing structures of a lithosphere can produce two outcomes: reactivation and reworking (Holdsworth et al., 1997, 2001). Reactivation is considered when there is a rejuvenation of some discrete structure, while reworking implies that a given volume of rock is strained, affected by metamorphic transformation and/or magmatism at least for a second time. However, a record of interfering structures and metamorphic imprints may result from a single protracted deformation phase (Carreras and Druguet, 2019) or from a sequence of tectonic events separated in time. In this regard, it is critical to have the absolute timing of deformation, to establish the similarity versus incompatibility of the stress fields required to produce the interfering structures, and whether the geometry of superimposed structures is conditioned by the previous record since the geometry and kinematics of reworking structures is not necessarily controlled by that of the previous ones. The volume of effect and penetrativeness of reworking processes are larger by comparison with those related to reactivation, which should be observed along discrete planes at the scale of analysis (Holdsworth et al., 1997).

Several factors can make a piece of the crust weak(er). These can be divided into primary/inherited ones and secondary ones. Inherited factors exist before the onset of a given deformation, whereas secondary factors emerge during that deformation. Once produced, secondary factors would mimic the effect of primary factors during a superimposed deformation event. Most common primary factors are composition, grain-size, and existence of primary anisotropies such as bedding (e.g. Baud et al., 2005). Temperature, pressure, fluid flow, grain-size reduction and recrystallization are among the most recognized weakening processes (e.g. Warren and Hirth, 2006; Cawood and Platt, 2021). All of

* Corresponding author.
E-mail address: diamor03@ucm.es (D. Moreno-Martín).

https://doi.org/10.1016/j.tecto.2022.229601
Received 8 June 2022; Received in revised form 7 September 2022; Accepted 28 September 2022
Available online 8 October 2022

the aforementioned factors can act together with others that are purely geometric, such as size (length, width and depth of a given anisotropy), orientation, interconnectivity and penetrativeness. The combination between all these factors, and how localized (discrete) versus broad are their weakening effects, would determine whether the crust is deformed by reactivating former anisotropies (e.g. a fault block moves once again) or is reworked by changing the internal structure of large pieces of it (Holdsworth et al., 2001).

The superposition of orogenic cycles is a defining characteristic of the lithosphere of the Iberian Peninsula. The Cadomian and Variscan orogens form part of the crystalline basement of Europe (Fig. 1), crop out in the west of the Iberian Peninsula and conforms the so-called Iberian Massif (Fig. 2). The Cadomian is an accretionary orogen formed in Ediacaran times in the periphery of Gondwana (Linnemann et al., 2014), whereas the Variscan Orogen resulted from the late Paleozoic collision of Gondwana, Laurussia and other pericontinental terranes located between both continents, after the closure of the Rheic Ocean and other marginal basins, to give rise to Pangea (e.g., Díez Fernández et al., 2016; Franke et al., 2017; Azor et al., 2019; Martínez Catalán et al., 2021). However, during the Alpine Orogen, the Iberian Massif belongs to the Iberian microplate, which has been subjected to deformation both along its margins (e.g., Pyrenees, Betics, Basque-Cantabrian chain; Vergés et al., 2002; Platt et al., 2013, García-Senz et al., 2019; Angrand and Mouthereau, 2021) and intraplate sections (e.g., Spanish-Portuguese Central System and Iberian Range; de Vicente et al., 2018; Aldega et al., 2019; Rat et al., 2019) since the latest Cretaceous, in its ongoing process of collision against the African and Eurasian plates during this orogeny (Kley and Voigt, 2008; Nocquet, 2012; Macchiavelli et al., 2017, and reference therein).

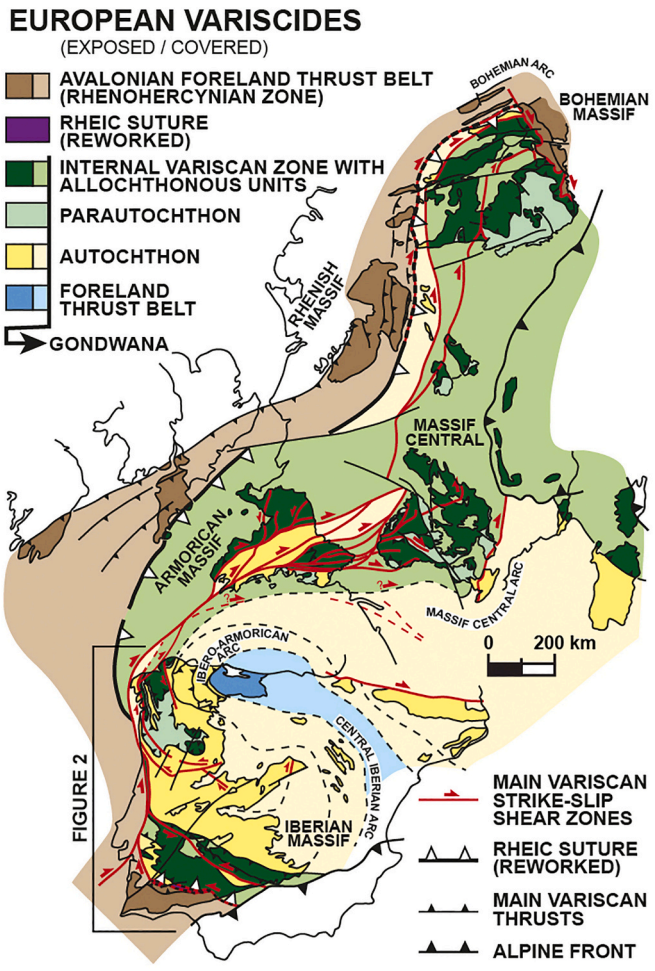

Fig. 1. Zonation of the Variscan Orogen after Díez Fernández and Arenas (2015). Location of the Iberian Massif (Fig. 2) is indicated.

The Spanish-Portuguese Central System is an Alpine intraplate mountain range (de Vicente et al., 2018) and its eastern sector includes a record that ranges from the Variscan (basement) to the Alpine orogenies. The Variscan record of its metamorphic basement has been studied by several authors (e.g., González Lodeiro, 1980; Fernández Rodríguez, 1991; Escuder Viruete et al., 1998; Rubio Pascual, 2013). This part of the Iberian Massif represents an internal section of the Variscan Orogen. The hinterland of this Paleozoic orogen in Central Iberia records alternating stages of crustal thickening and attenuation (Díez Balda et al., 1995; Díez Fernández et al., 2013; Rubio Pascual et al., 2013; Díez Fernández and Pereira, 2016). This alternation had not been recognized in the basement of the eastern sector of the Spanish-Portuguese Central System, which remained a section of the Variscan Orogen unaffected by processes related to crustal thinning. Additionally, this exposure of Variscan basement occurs within the core of an Alpine mountain range that exceeds 2500 m in height above sea level (1800 m in the study area). Most of the internal structure of this basement has been attributed to the Variscan cycle (González Lodeiro, 1980; Fernández Rodríguez, 1991), although some works have suggested a Permian and also Alpine age for some faults (Fernández Rodríguez, 1990; de Vicente et al., 2009, 2018, 2021; Angrand et al., 2020). Yet, an analysis focused on identifying reactivation and/or reworking processes in this area was missing.

In this work we analyze the structure of a representative sector of the easternmost part of the Spanish-Portuguese Central System aiming to identify the interference between the whole set of structures. We discuss the nature and extent of reworking processes that are linked to each orogeny, with particular emphasis on deciphering the role of previous structures in how continental crust accommodates subsequent deformation. The compositional and structural inheritance is analyzed together with regional stress and thermal structure to explain the geometry, kinematics, distribution (including penetrativeness), and reactivated character of individual structures. Our main objective is to provide a case example about reworking and reactivation for all contractional, strike-slip and extensional structures in an Alpine intraplate mountain range that holds evidence of previous Permian extensional tectonics and an even older record of Variscan continental collision.

2. Geological setting

The study area is located in the Spanish-Portuguese Central System, which is an intraplate mountain range raised during the Cenozoic (Oligocene-Lower Miocene) and containing pieces of Ediacaran and Paleozoic metamorphic basement (Fig. 3; de Vicente et al., 2018). The basement of Central and Western Europe includes relicts of the Variscan Orogen (Fig. 1). This orogen was formed in relation to the assembly of Pangea, after the collision between Gondwana, its pericontinental terranes and Laurussia during the Devonian and Carboniferous (Matte, 2001; Franke et al., 2017; Martínez Catalán et al., 2021). The Iberian Massif (Fig. 1) represents a portion of that orogen and has been divided into different geotectonic and paleogeographic domains (Fig. 2; Díez Fernández and Arenas, 2015). We focus on an area in the easternmost part of the Central Iberian Zone (Figs. 2 and 3).

The Central Iberian Zone represents most of the Iberian Autochthon (i.e., Gondwana *s.s.*; Fig. 2), which underlies a set of peri-Gondwanan allochthonous nappes (Martínez Catalán et al., 2007; Ribeiro et al., 2007; Simancas et al., 2013; Díez Fernández et al., 2016). The Variscan record of the Central Iberian Zone combines folds and faults formed during contractional stages with domes and structural basins, generation of anatectic granitoids and normal faults resulting from gravitational collapse and syn-orogenic extension (Escuder Viruete et al., 1994; Gómez Barreiro et al., 2010; Díez Fernández et al., 2012; Rubio Pascual et al., 2013; Martínez Catalán et al., 2014; Azor et al., 2019). Its Variscan structure results from early crustal thickening produced during the

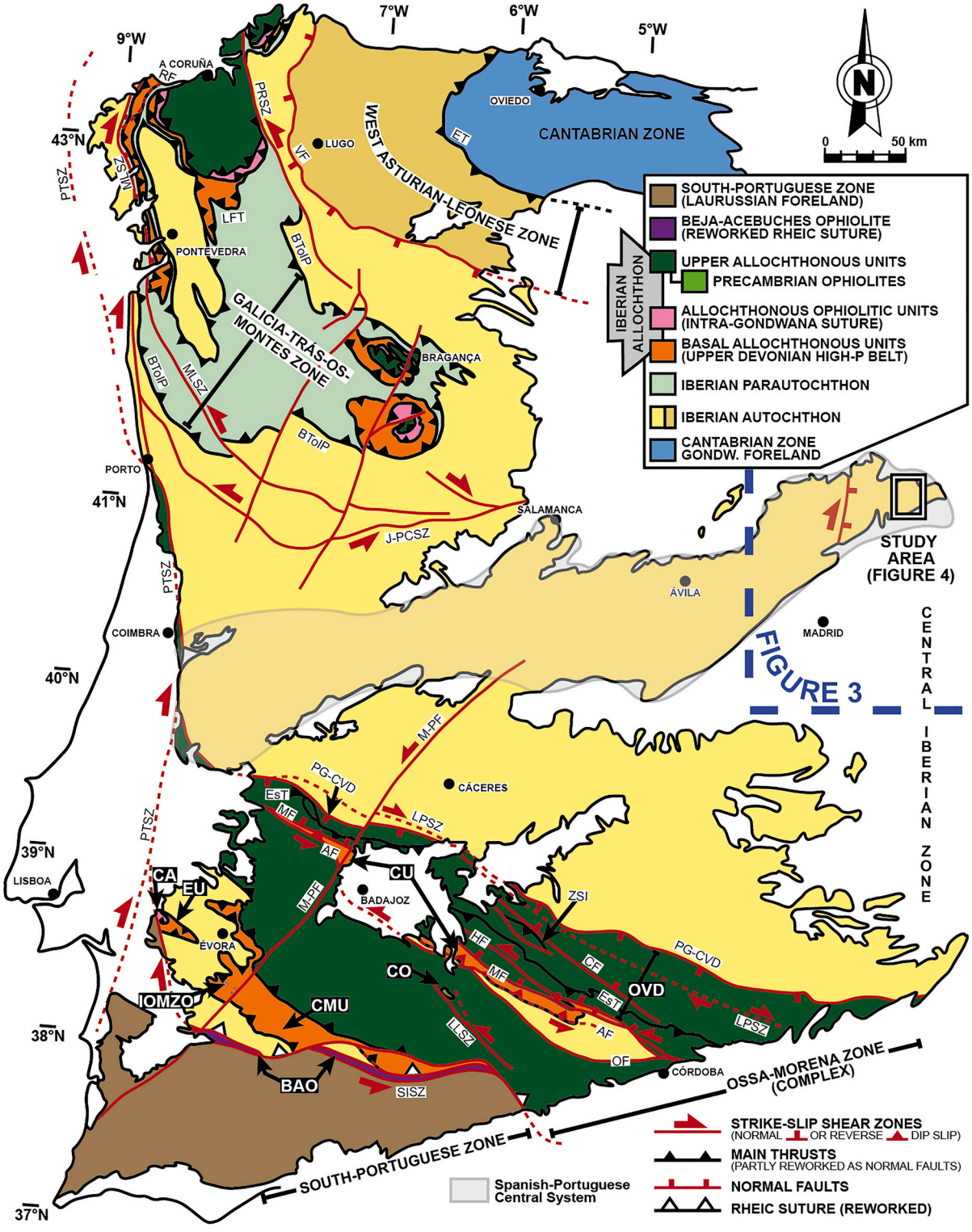

Fig. 2. (a) Zonation and major tectonic elements of the Iberian Massif after Díez Fernández and Arenas (2015). Location of the maps in Figs. 3 and 4 is indicated. Abbreviations: AF — Azuaga Fault; BToIP — Basal Thrust of the Iberian Parautochthon; BAO — Beja–Acebuches Ophiolite; CA — Carvalhal Amphibolites; CF — Canaleja Fault; CMU — Cubito–Moura Unit; CO — Calzadilla Ophiolite; CU — Central Unit; EsT — Espiel Thrust; EU—Escoural Unit; ET—Espina Thrust; HF—Hornachos Fault; IOMZO —Internal Ossa-Morena Zone Ophiolites; J–PCSZ — Juzbado-Penalva do Castelo Shear Zone; LFT — Lalín-Forcarei Thrust; LPSZ — Los Pedroches Shear Zone; LLSZ — Llanos Shear Zone; MLSZ — Malpica–Lamego Shear Zone; M–PF — Messejana – Plasencia Fault; MF — Matachel Fault; OF — Onza Fault; OVD — Obejo–Valsequillo Domain; PG–CVD — Puente Génave–Castelo de Vide Detachment; PRSZ— Palas de Rei Shear Zone; PTSZ — Porto–Tomar Shear Zone; RF — Riás Fault; SISZ —South Iberian Shear Zone; VF — Viveiro Fault; ZSI — Zalamea de la Serena Imbricates.

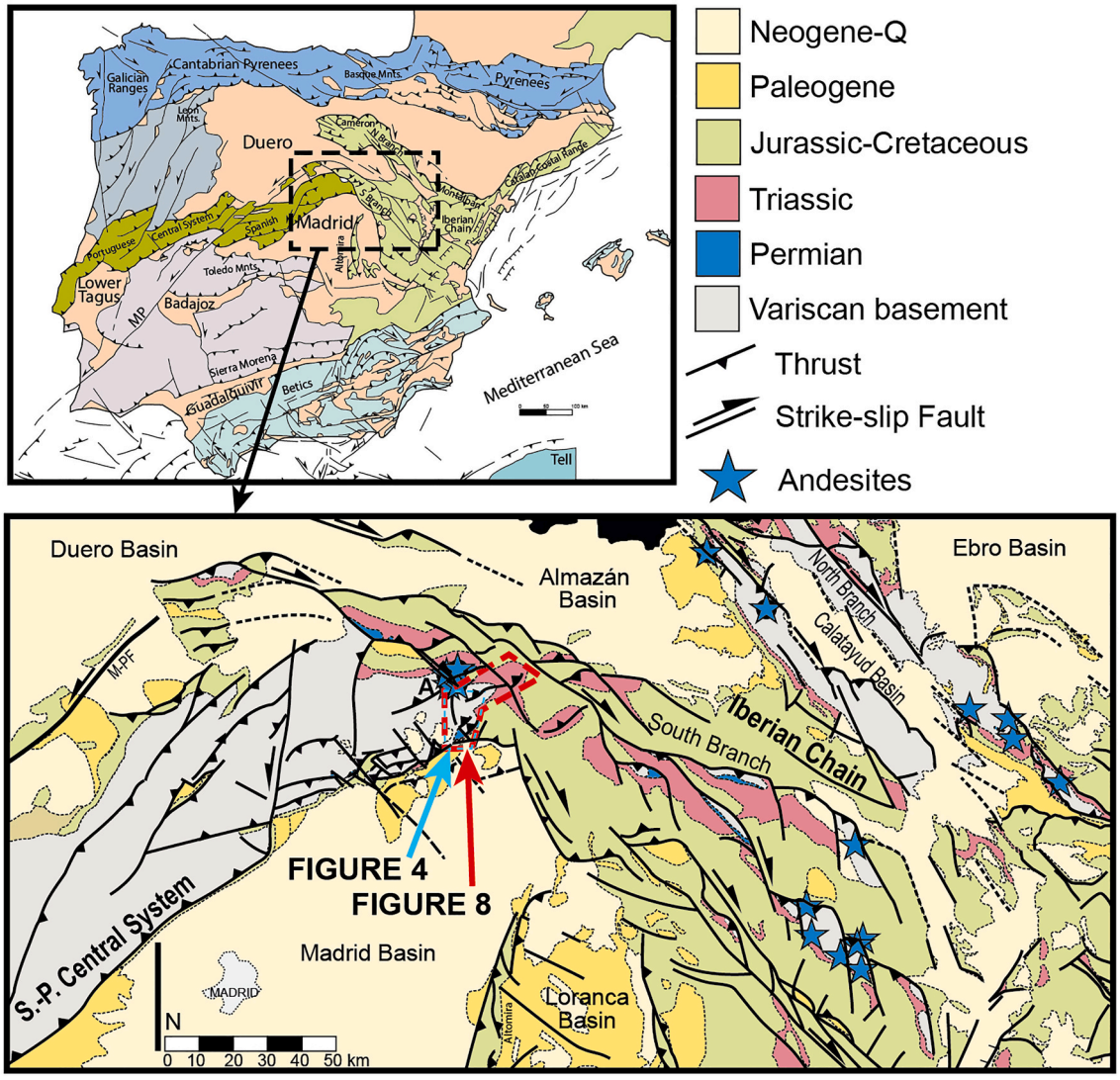

Fig. 3. Regional tectonic map showing the main Alpine basins (brown) and mountain ranges (other colors) of the Iberian Peninsula (on top), with an inset to the eastern part of the Spanish-Portuguese Central System (below). Location of the map in Figs. 4 and 8 is indicated. Abbreviations: A — Atienza andesites; M–PF — Messejana–Plasencia Fault. (For interpretation of the references to colour in this figure legend, the reader is referred to the web version of this article.)

transference of the allochthonous nappes onto it (D_1), followed by the collapse and extension of the orogen (D_2) that alternated with the development of intra-continental strike-slip shear zones (D_3) and orocline formation (Martínez Catalán et al., 2007; Gutiérrez-Alonso et al., 2015; Díez Fernández et al., 2016).

In the section of the Central Iberian Zone that crops out in the basement of the Spanish-Portuguese Central System (Fig. 3), early Variscan folding and thrusting thickened the crust (D_1; Bellido et al., 1981; Capote et al., 1981; Macaya et al., 1991; Rubio Pascual et al., 2013). The subsequent development of extensional shear zones and coeval magmatism conducted the gravitational and thermal reequilibrium during a stage of crustal thinning (D_2; Doblas, 1991; Doblas et al., 1994; Hernaiz Huerta et al., 1996; Rubio Pascual et al., 2013; Arango et al., 2013), which was followed by a new stage of moderate crustal thickening driven by strike-slip shear zones and related upright folds (D_3; Martínez Catalán, 2011; Arango et al., 2013). The Variscan structural record of the study area (Fig. 4; see location in Fig. 2) so far described includes a train of *E*-verging folds, underneath which is a ductile shear zone acknowledged as a thrust, plus a set of upright folds that bent all of the previous structures (González Lodeiro, 1980; Fernández Rodríguez, 1991). This underlying ductile shear zone has a minimum thickness of 7 km, which is comparable in thickness to flat-lying or shallowly-dipping ductile shear zones that are key to understanding the evolution of collisional orogenic systems, such as the western Grenville Orogen (Jamieson et al., 2007) or the Himalayas (South Tibetan detachment; Beaumont et al., 2001).

The Spanish-Portuguese Central System shows thick-skinned, and locally a thin-skinned with basement involved, tectonic styles and thin sedimentary cover (Fig. 3; de Vicente et al., 2018). The crustal structure of this Cenozoic mountain range resembles an asymmetric, crustal scale pop-up (de Vicente et al., 2018). At the southern boundary, along the northern margin of the Madrid Cenozoic foreland basin, Alpine deformation is mainly concentrated in a single reverse fault that cuts through the entire crust with a Moho throw of 3–5 km (Andrés et al., 2019, 2020), while to the north and defining the southern margin of the Duero Cenozoic foreland basin, Alpine deformation is distributed in several reverse faults with smaller throw (de Vicente et al., 2018). Alpine reverse faults are accompanied by strike-slip faults, which are generally left-lateral if they strike N-S to NNE-SSW or right-lateral if they strike NW-SE to NNW-SSE (de Vicente et al., 2007). The S (Castilian) Branch of the Iberian Range, to the E, constitutes a right-lateral mega tear strike-slip deformation belt that laterally accommodated the uplift of the Spanish-Portuguese Central System (de Vicente et al., 2009). Out of this scheme, the Messejana-Plasencia fault, a NE-SW left-lateral strike slip

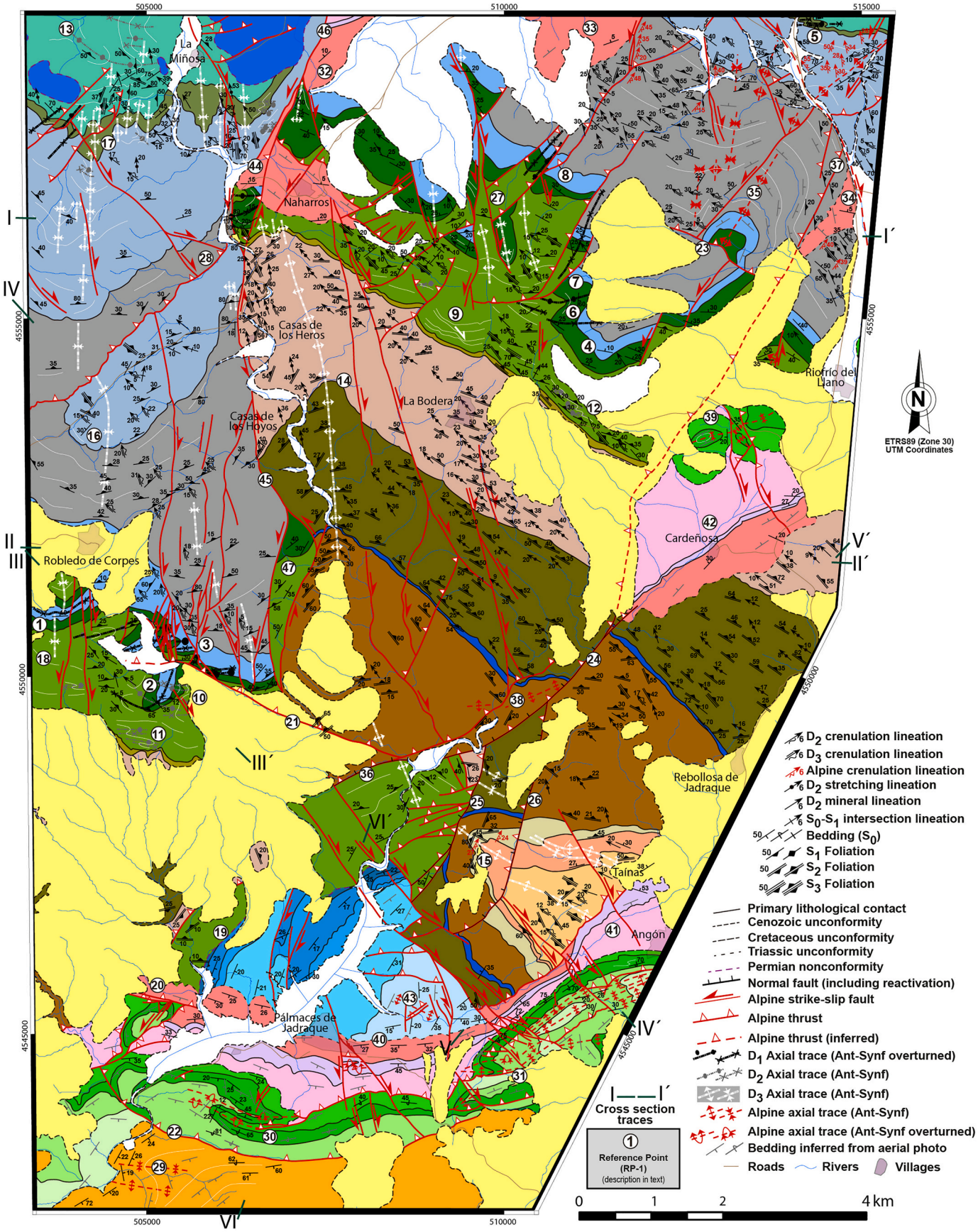

Fig. 4. Geological map of the study area. The lithological legend is shown in Fig. 5.

fault, parallel to the main thrusts with simultaneous movement, has been explained as a deformation partition process that accommodated a generalized N-S shortening (de Vicente et al., 2018).

This study has been carried out in the easternmost part of the Spanish-Portuguese Central System (Figs. 2 and 3 include the location of the study area shown in Fig. 4). This area contains Permian sedimentary basins as well as Triassic and Cretaceous sedimentary rocks that crop out as isolated outcrops between basement metamorphic rocks that belong to the Central Iberian Zone of the Iberian Massif (Sopeña, 1979) (Figs. 4 and 5). The Permian basins are bounded by normal and strike-slip fault systems (Fernández Rodríguez, 1990). Jurassic sediments are lacking and the Upper Cretaceous series rest on top of the Triassic rocks. Cenozoic syn-orogenic deposits of the northern boundary of the Madrid Cenozoic foreland basin occur to the south. Younger Late Cenozoic low-dipping piedmonts, fluvial and alluvial Quaternary deposits occur as patches over all of the bedrock. An extended description of the lithostratigraphy of the study area is included as supplementary data (SD-1). The geological map in Fig. 4 and the cross-sections in Fig. 5 show a

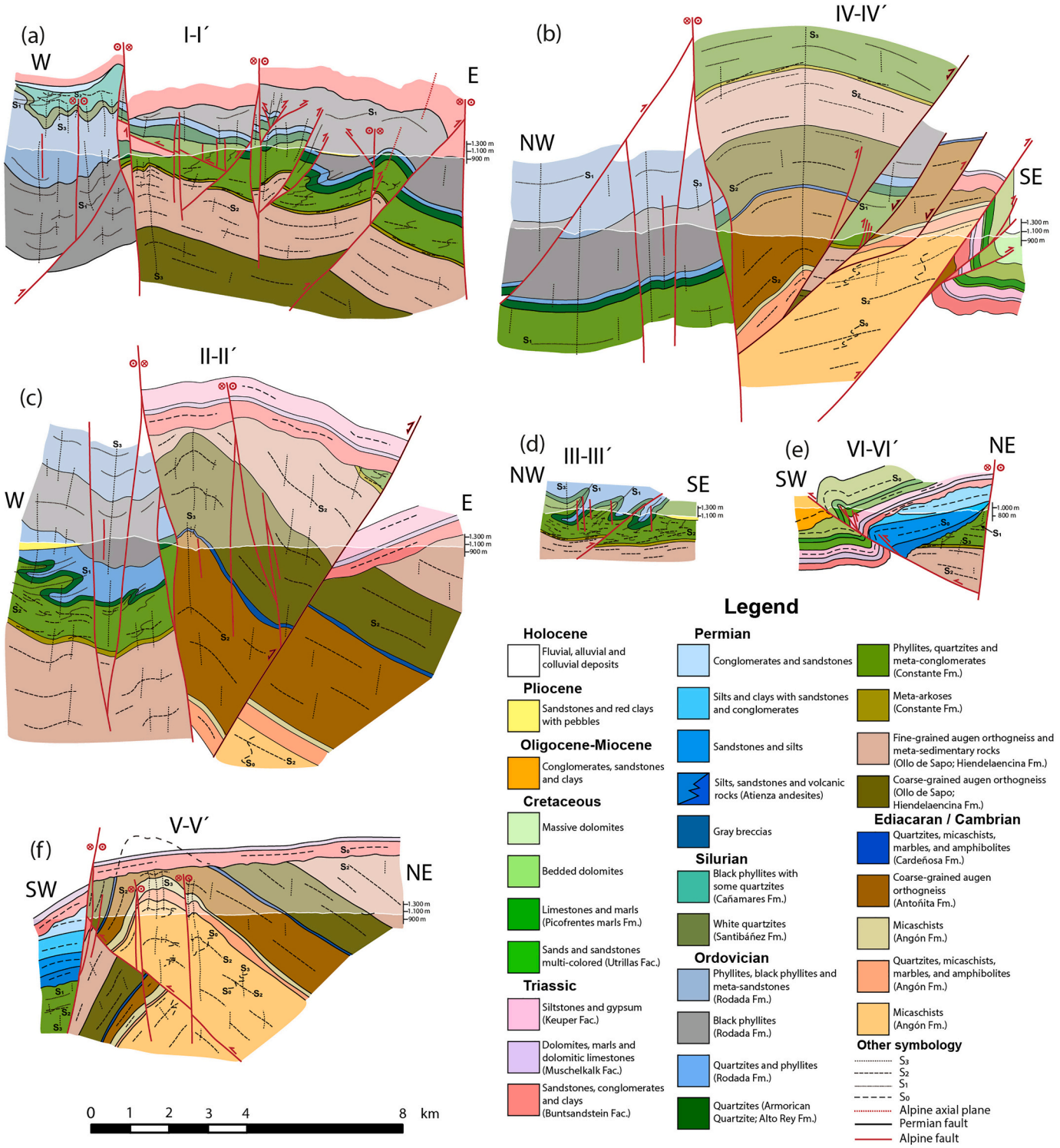

Fig. 5. Cross sections showing the main structures. Their traces are shown in Fig. 4.

graphical presentation of the main relationships between lithostratigraphical units.

3. Materials and methods

Geological mapping was performed at the 1:25,000 scale, with the exception of well exposed sections (road cuts), which were mapped at the 1:10,000 scale to obtain a higher resolution to analyze structural relationships. Topographic maps and digital orthophotos from the Spanish National Geographical Survey (http://centrodedescargas.cnig.es) were used as base maps. The structural analysis and representation of structural data in stereographic plots were carried out using Geo-Calculator v. 5.0.4 (R. Holcombe; https://www.holcombe.net.au/software) and Stereonet v. 11.3.1 (R.W. Allmendinger, https://www.rickallmendinger.net/stereonet; Cardozo and Allmendinger, 2013). For the presentation of structural data, such as primary geometrical features and relationships with previous and subsequent structures, we have selected domains where individual structures are best preserved (to define primary geometries) or crosscutting relationships are easily observed (to define interference patterns). These domains are referred to as Reference Points (RP) throughout the text.

In order to constrain petrological and qualitative metamorphic evolution as well as microstructural features like foliation sequences and kinematic criteria, 14 samples were collected for petrographic analyses. Thin sections were prepared normal to foliation and parallel to lineation (Means et al., 1980; Díaz-Azpiroz et al., 2019), but in cases with penetrative crenulation lineation, the thin sections were done normal to axial planes and fold axes. A summary of petrographic observations is presented as a blastesis-deformation diagram (SD-2; Supplementary data 2).

The calculation of the orientation of principal stresses was performed in two different ways. In an Alpine fault zone, we used a fault population of fault-slickensides couples to calculate the stresses by means of the stress inversion method following Michael (1984) and Vavryčuk (2014). In an exposure including minor Variscan faults and related tension gashes, the kinematics and orientation of principal stresses were calculated following Angelier (1979).

4. Results

4.1. Variscan structural data

The crystalline basement of the study area (Fig. 4 and Fig. 5) has been affected by three phases of deformation (D_1, D_2 and D_3), each of them associated with metamorphism (M_1, M_2 and M_3) and foliation development (S_1, S_2 and S_3).

4.1.1. D_1 folds and fabrics

The main D_1 structures are a fold train and an axial plane foliation. At a regional scale, this planar fabric is the first one recognizable in chronological order, so it will be referred to as S_1.

D_1 folds are observed at several scales. Macroscopically, they are best preserved towards the northern sectors of the study area. A good example is the fold train south of Robledo de Corpes (Reference Points (RP)-1, 2, and 3; Fig. 4; Fig. 5d). Some of these folds can be observed in aerial photography (SD-3b and c). Other examples are found NE of La Bodera (RP-4; Fig. 4; Fig. 5a) and in Silurian rocks exposed in the NE part of the study area (RP-5; Fig. 4; Fig. 5a). The geometry of D_1 folds varies between overturned (RP-2; Fig. 4; Fig. 5d) and recumbent (RP-1, 4 and 5; Fig. 4; Fig. 5c). D_1 folds are asymmetric, with backlimbs bearing lithostratigraphic series in normal position (e.g., RP-1 and 4; Fig. 4), and forelimbs with series in upright or reversed position (e.g., RP-2 and 6; Fig. 4). D_1 fold vergence is to the E, as inferred from the location of backlimbs (RP-7 and 8; Fig. 4) relative to forelimbs (RP-6; Fig. 4) (Figs. 5 a, c and d).

S_1 is parallel to the axial plane of D_1 folds. The local orientation of D_1 fold axes (F_1), calculated from S_0-S_1 intersections, ranges between NE-SW, N-S and NW-SE trends, with a plunge direction to the NW (21°/300°; Fig. 6a). S_1 is associated with a mineral lineation defined by muscovite, biotite and quartz (10°/305°). S_1 is also related to a stretching lineation marked by stretched clasts in meta-sandstones and meta-conglomerates (10°/300°).

Evidence of S_1 development is found all across the crystalline basement. S_1 either defines the local main foliation or be a relict fabric. As a relict fabric, S_1 can be preserved as an internal foliation (S_i) within post-S_1 porphyroblasts, or as an external (and usually microfolded) fabric in microlithons related to subsequent foliation.

The nature of S_1 varies depending on lithology. In meta-sandstones, S_1 is a spaced cleavage defined by biotite, muscovite and aggregates of opaque minerals and by the preferred orientation of flattened quartz and feldspar grains. In metapelites, S_1 ranges from phyllitic cleavage to continuous schistosity with lepidoblastic to grano-lepidoblastic texture defined by the preferred orientation of quartz, muscovite, biotite, chlorite, and minor amounts of tourmaline, plagioclase, opaque minerals, and rare garnet (SD-4a and b). In the orthogneisses and the paraderived rocks that are interspersed with and below them, S_1 is never the main foliation, but a fabric either within porphyroblasts and/or preserved in microlithons. In these sections, the first foliation in the metasedimentary rocks (S_1) appears as an internal schistosity (S_i) defined by micro-folded inclusions of quartz, muscovite, biotite, and opaque minerals within garnet porphyroblasts (SD-4c, d, and e). In ortho-derived rocks, S_1 occurs as microfolded fabric relicts loosely defined by biotite and muscovite within quartzofeldespathic microdomains, or defining an internal microfolded fabric within garnet porphyroblasts that includes quartz, biotite, and opaque minerals (SD-4f, g, h and i).

4.1.2. D_2 fabrics and related structures

The main D_2 structures are discrete brittle-ductile and brittle shear zones, overturned to recumbent folds, and a foliation with (inferred) primary flat-lying geometry that parallels the axial plane of said folds. At a regional scale, this foliation is the second in chronological order and will be referred to as S_2.

D_2 brittle-ductile shear zones cut D_1 structures and are restricted to pre-Variscan lithologies structurally above the fine-grained Ollo de Sapo Formation. The thickness of these shear zones ranges between 2 and 3 mm and up to several meters. The thinner examples are recognizable at the outcrop scale (SD-3d), while the thicker ones (including the drag folds they produce) can be observed in aerial photography (SD-3e) (RP-9; Fig. 4). Mean orientation of shear planes is 008°/36° (Fig. 7a), although some conjugate pairs do exist. These shear zones occur together with sub-vertical tension gashes and sub-vertical sigmoidal veins (Fig. 7a), mainly filled with quartz and usually localized within most competent layers (e.g., in meta-sandstones intercalated between metapelites; SD-3f). Some of these shear zones are filled with quartz, feldspar, and lesser amounts of muscovite. The brittle-ductile shear zones locally connect with boudin necks formed after stretching of meter-scale domains subparallel to S_0 and S_1 (SD-5a). Both the brittle-ductile shear zones and boudin necks can share infilling. Veins are nearly concordant with the boundaries of the hosting shear zone and can show sigmoidal structure coherent with the kinematics of its host. Dominant kinematics of these shear zones is top-to-the ESE, as inferred from offsets of strata (SD-5b), drag folds (SD-5c), sigma structures formed at the expense of layers of strata, sigmoidal structure of veins, SC structures and C′ structures (SD-5d). Such kinematics, combined with the orientation of their shear planes (dip direction towards ESE), results in shear zones with normal fault geometry.

In the pre-Variscan rocks atop the Ollo de Sapo Formation, D_1 folds and S_1 are affected (refolded) by overturned to recumbent (D_2) folds with axial planes markedly oblique to those of D_1 folds. D_2 axial planes are low-dipping and usually with a dip-direction towards the N (Fig. 6c) (RP-10; Fig. 4). This type of folds occurs both at outcrop (SD-5e),

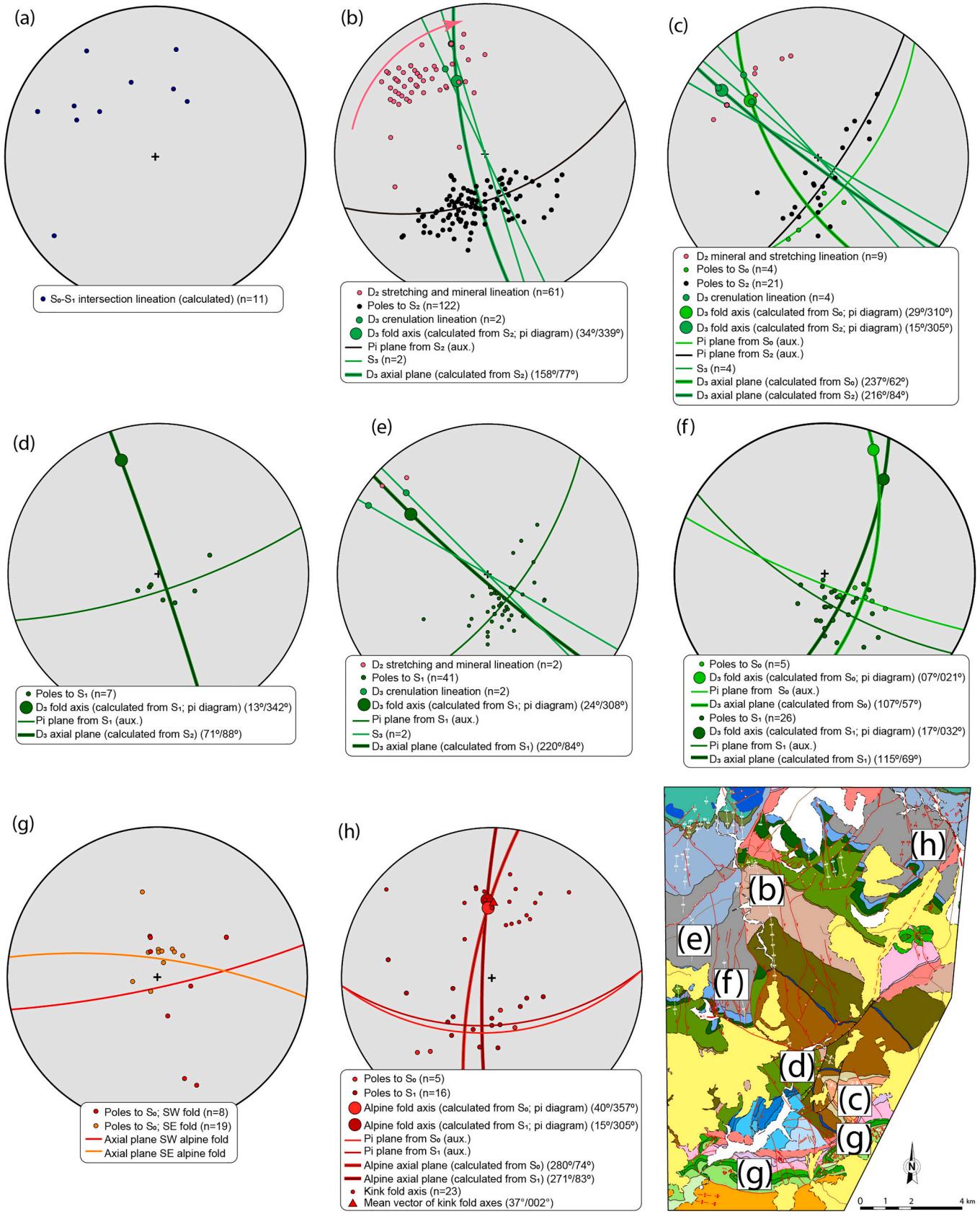

Fig. 6. Stereograms with structural data. The companion map shows the approximate location of the areas analyzed in each diagram. a) S_0-S_1 intersection lineation, representing the axes of D_1 folds. b) S_2 planes and associated mineral and stretching lineation. All of them are affected by D_3 folds (note the reorientation of D_2 lineations towards the axis of the calculated D_3 fold, as indicated by a red arrow). Representation of geometric elements (measured and calculated) related to D_3 folds and located in different parts of the study area: c) SE area; d) central zone; e) WNW zone; f) W zone. Representation of geometric elements of the Alpine folds located at g) S and h) NE of the study area. (For interpretation of the references to colour in this figure legend, the reader is referred to the web version of this article.)

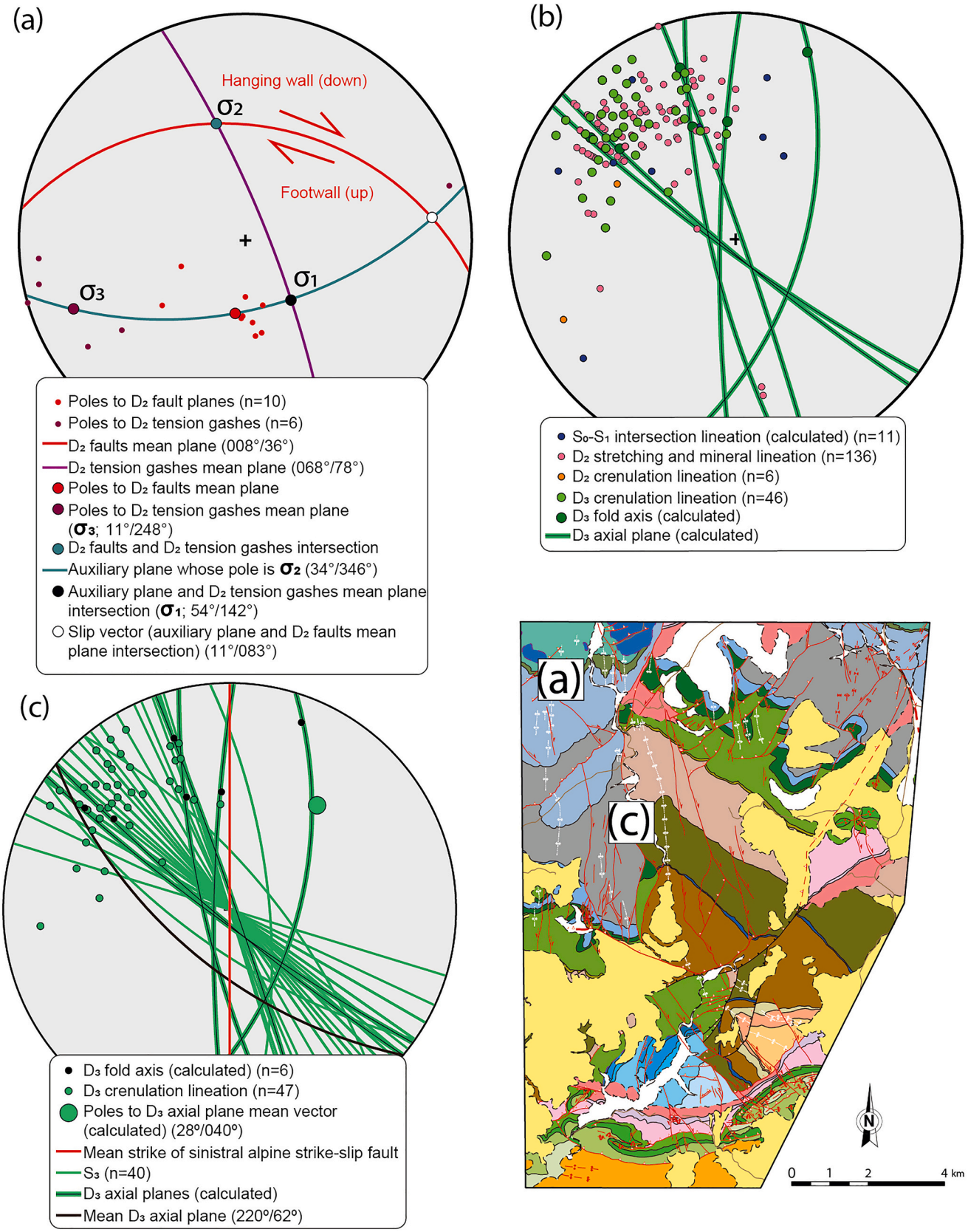

Fig. 7. Stereograms with structural data. The companion map shows the approximate location of the areas analyzed in each diagram. a) Calculation of the orientation of the D_2 principal stress axes using faults and associated tension gashes (following Angelier, 1979). b) D_1, D_2 and D_3 linear structures showing similar dispersion in orientation (it includes data from the whole study area). c) Axial planes of D_3 folds faced against the trend of the main Alpine sinistral strike-slip fault that appears in the western sector of the study area to show their regional obliquity.

hectometer (SD-5f) (RP-10, 11 and 12; Fig. 4), and up to the kilometer scale (RP-13; Fig. 4). The regional trend of the axes of these folds, inferred from mapping of their axial traces, varies between *E*-W and NW-SE (Fig. 4). These structures can develop local thickening of their hinge zone and thinning along their limbs, being greater in the case of short limbs (SD-5f) (RP-12; Fig. 4). Local thinning (shearing) in short limbs can also be accompanied by offsets of strata along discrete top-to-the-ESE shear zones. Folds with a geometry similar to those described above can also be observed in the Ollo de Sapo Formation and underlying lithologies. However, the reference planes to observe them in the field do not include S_1 (not visible at a mesoscopic and macroscopic scale). In these cases, D_2 folds are deduced from primary compositional banding, such as bedding (S_0) in micaschists (SD-5e) and xenoliths in metagranites, or from other types of secondary structures, such as dikes or quartz veins (SD-5 g). The fold axis trend measured in these structures (10°/305°) is equivalent to the one inferred from axial trace analysis atop the Ollo de Sapo Formation.

D_2 folds can be symmetric (SD-5 g) or asymmetric (SD-5e). Asymmetric D_2 folds are more abundant than symmetric ones upwards from the top of the Ollo de Sapo Formation, and downwards from the base of that same formation. However, dominant fold asymmetry is different at each structural level. Atop the Ollo de Sapo Formation, D_2 folds define ESE-verging fold trains (RP-11 and 12; Fig. 4) (SD-5f), with the lithostratigraphy in normal position. Below the Ollo de Sapo Formation, D_2 fold asymmetry is usually opposite to that of the upper structural levels. However, in layered metasedimentary rocks at the lowest structural levels (e.g., Angón Formation), D_2 fold hinges in asymmetric structures are thicker than its contiguous limbs, and the short limbs (expected to be forelimbs) are also thicker than the long limbs (expected to be backlimbs). Fernández Rodríguez (1991) made similar observations in quartz veins within the Ollo de Sapo Formation. The (D_2) fold asymmetry in these cases was likely reversed by progressive heterogeneous simple shearing (Carreras et al., 2005).

S_2 transposes S_1 to a variable extent, depending on the distribution and type of superimposed foliation. S_2 is heterogeneously distributed in the region. S_2 is the main foliation and generally the only one recognizable with the naked eye downwards from the top of the Ollo de Sapo Formation. On the other hand, S_2 can be potentially observed at any structural level upwards from the top of the Ollo de Sapo Formation, but it never concentrates along specific bands nor is S_2 the main local foliation (S_1 always is). S_2 is subparallel to the axial plane of D_2 folds in all cases (SD-5e and g).

S_2 shows different characteristics depending on the lithology and structural level of observation. Atop the Ollo de Sapo Formation, S_2 occurs as a variably evolved crenulation cleavage formed at the expense of S_0 and S_1. Different stages of development to form a new foliation are observed, from incipient crenulation through to metamorphic differentiation in crenulation septa and growth of new mica, transposition of relict S_1 in microlithons, and the eventual development of a new D_2 foliation. Structures associated with the development of S_2 cleavage can be symmetric, asymmetric, or define C—S structures (SD-5 h). S_2 cleavage is more common near D_2 brittle-ductile shear zones and is accompanied by a crenulation lineation trending 15°/300°. S_2 cleavages are defined by reoriented S_1-minerals towards septa (mainly quartz, white mica, biotite, opaque minerals) and by recrystallization and growth of quartz, white mica, biotite and chlorite. The growth of biotite blasts subparallel to S_2 is markedly bimodal. On the one hand, there are biotite blasts with a size equivalent to that of S_1-biotite. On the other hand, there are post-S_1 biotite porphyroblasts parallel to S_1 and S_2, but significantly larger in size than any other biotite crystal in the rock, sometimes with more than 20 times the size of S_1-biotite (SD-4j and k). At both a mesoscopic and microscopic scale, S_2 crenulation cleavages generate secondary compositional banding (SD-4a), which defines most of the main foliation from the Ollo de Sapo Formation downwards (SD-4c and d).

From the Ollo de Sapo Formation downwards, S_2 is a schistosity in the metapelites (SD-6a), a spaced foliation in the quartzites and other meta-sandstones (SD-6b), and a gneissic banding in all types of orthogneiss (SD-6c and d). In all cases, S_2 is parallel to a compositional banding, which is secondary in origin for the metaigneous rocks (gneissic banding) and usually composite (primary plus secondary) in the case of paraderived lithologies.

The main foliation (S_2) in micaschists is defined by a millimeter-scale alternation of quartz-rich and mica-rich layers that show porphyrogranolepidoblastic texture (SD-4c and d). The quartz-rich layers are composed of quartz and minor muscovite, biotite, and plagioclase. The mica-rich layers mainly include muscovite and biotite, with variable amount (always accessory) of garnet, staurolite, kyanite, sillimanite, tourmaline, opaque minerals and zircon. Garnet appears as subidiomorphic porphyroblasts up to 1 cm in length. Garnet can show slightly elongate shape parallel to the main foliation. The main foliation wraps around garnet and shows anastomosed structure. This fabric can also be included towards garnet rims, where it shows continuity respect to external foliation (SD-4e). These mineral inclusions in garnet should not be confused with S_1 microinclusions, which do not show continuity with external foliation and appear micro-folded (see description above). Kyanite occurs as idiomorphic to subidiomorphic porphyroblasts lacking internal foliation and are surrounded by fibrous-looking mineral masses (now retrograde to sericite) that probably represent former sillimanite aggregates (SD-4 l). Kyanite can sometimes show slightly elongate shape subparallel to the main foliation. Staurolite appears as porphyroblasts up to 3 mm in length and with a tendency to be subidiomorphic to allotriomorphic. The orientation of the long axis of staurolite with respect to the main foliation varies from subconcordant to virtually perpendicular. The main foliation anastomoses around these porphyroblasts (preferably if its long axis is subconcordant with the main foliation), or it is included within them and in continuity with the external foliation (SD-4 m). Pressure shadows made of the same minerals that define the main foliation can be seen around any of the porphyroblasts in the micaschists.

Most features of the main foliation (S_2) are common to the different types of orthogneiss (see extended description by Fernández Rodríguez, 1991). The main foliation in orthogneisses is defined by the preferred orientation of individual crystals of quartz, K-feldspar, plagioclase, biotite, muscovite, sillimanite, and opaque minerals. This mineralogy is arranged as alternating bands (gneissic banding) that also define the main foliation. There are bands richer in quartz, K-feldspar and plagioclase that are up to 1 cm thick, which alternate with thinner bands (few mm thick) that are richer in melanocratic minerals, such as those mentioned before, plus non-individually oriented monazite, zircon, allanite, and occasionally garnet. Lateral continuity of the compositional bands is limited, few cm at most, and anastomosis between melanocratic bands is common. Garnet usually occurs as porphyroblasts (with internal fabric) in gneisses of the Ollo de Sapo Formation (SD-4f, g, h and i), whereas in the rest of the orthogneisses garnet crystals make part of the granoblastic texture. Any variety of orthogneiss contains porphyroclasts of greater or lesser size, either derived from quartz (e.g., Ollo de Sapo Formation) and/or K-feldspar phenocrysts (e.g., any of the augen orthogneisses) (SD-4n and o). In most cases, the porphyroclasts show elongate shape sub-concordant with the main foliation (SD-4f, g, h, i, n and o), which wraps around them. Porphyroclasts usually present pressure shadows formed by the same mineralogy that defines the main foliation.

Minerals grown during the development of S_2 show preferred linear orientation along foliation planes and define a mineral lineation. In metapelites, this lineation is defined by garnet and staurolite (if elongate), by pressure shadows around porphyroblasts, and by micas, quartz, sillimanite and tourmaline. In meta-sandstones, quartz and feldspar show elongate shape on S_2 planes, defining a stretching lineation (individual mineral grains are interpreted to be sedimentary clasts). In the orthogneisses, a mineral lineation is mainly defined by preferred orientation of micas. However, all types of orthogneiss contain stretched

porphyroclasts, whose long axes are aligned and define a stretching lineation on S_2 planes (SD-4 l and m). Additionally, microdomains rich in felsic minerals and aggregates of melanocratic minerals show elongate shape on S_2 planes and conform to the orientation of the stretching lineation. Mineral and stretching lineations related to S_2 are parallel in all the lithologies. Their regional trend ranges between NW-SE and N-S, with a plunge to the N (Fig. 6b).

The development of S_2 goes hand in hand with the formation of asymmetric microstructures defined both by individual minerals and by mineral aggregates. Sigma (SD-6c) (the most abundant) and delta-type objects have been observed in porphyroclasts in augen orthogneisses and in porphyroblasts of the micaschists. S—C (SD-5d) and C′ fabrics are common in orthogneisses and metapelites (SD-5 h), whereas asymmetric (sigmoidal) pressure shadows and asymmetric folds are abundant in the micaschists (SD-5e). The majority of individual observations indicate top-to-the-SSE sense of shear, although some local data pointed to the opposite sense, i.e. to the NNW.

4.1.3. D_3 folds and fabrics

The bedding (S_0), S_1, and S_2 are jointly affected by folds (Fig. 4; Fig. 5a, b, c, e, and f). Although there are different families of folds that affect these fabrics, this section focuses on the folds exclusive to the basement rocks (SD-6e), so it can be excluded that they could represent post-Variscan deformation. These folds constitute a third phase of Variscan deformation (D_3). In the geological map (i.e., at a regional scale), D_3 folds can be recognized from the curved structure of S_2. Good examples can be observed in any section dominated by S_2, for instance, in lithologies below the top of the Ollo de Sapo Formation (RP-14 and 15; Fig. 4) (Figs. 6b and c). D_3 folds can also be observed above that structural level at the macroscale, but formed at the expense of S_1 and S_0 in the absence of D_2 structures (RP-16, 17 and 18; Fig. 4) (Figs. 6d, e and f). The recognition of D_3 folds at the mesoscale (SD-6e) and microscale (SD-4a, b, j and k) is based on the same criteria.

D_3 folds are upright and their axes plunge consistently to the N (RP-14; Fig. 4). Tightness of D_3 folds based on interlimb angle varies between closed (30°) and gentle (120°), the open type (70°) being the most common (Figs. 5b, c and f). Fold axial planes generally strike NW-SE (Figs. 4, 6b, c, d and e), but it varies slightly towards a N-S and NN*E*-SSW direction in the central sector (RP-14; Fig. 4) (Fig. 6f). D_3 fold axes trend varies between N-S and NW-SE, with rare cases trending E-W.

D_3 folds produce a crenulation lineation at the expense of S_0, S_1 and/or S_2 (SD-6a). This lineation is more penetrative in phyllitic and schistose rocks and usually occurs alongside a subvertical crenulation cleavage (S_3). S_3 is defined by pre-D_3 minerals reoriented to septa and by the preferred orientation of newly formed muscovite, quartz, chlorite and sericite parallel to cleavage planes (M_3; SD-4a, b, j and k). S_3 is locally defined by biotite porphyroblasts (M_3; SD-4j). These blasts can even trap former tectonic fabrics (e.g., S_1) affected by D_3 folds (SD-4 k).

4.2. Post-Variscan structural data

Most lithological units in the study area are affected by faults. Yet, outcrop conditions allowed only one fault zone to be observed during this study, so there are uncertainties regarding the kinematic history of many individual faults. Based on the geometry and current relative separation between rock formations at each side of the faults deduced from the mapping of lithologies and previous structures, we establish three main fault groups: strike-slip, reverse and normal faults. This classification does not exclude the possibility that some fractures are oblique-slip faults, but we will focus on the dominant type of slip (dip-slip vs. strike-slip) for description purposes.

There are folds that affect the post-Variscan cover (Fig. 4), so there is the potential that the Variscan basement is affected by these folds too. A preliminary analysis observing the post-Variscan structure just in the cover indicates these folds trend E-W to NE-SW.

4.2.1. Permian structures: direct observations and inferences

Normal faults and strike slip faults are generated during the Permian extension. Normal faults seem more abundant in sections nearby Permian rocks. The V-shapes of the map trace of the northwestern boundary of the Permian series (RP-19; Fig. 4) indicates it dips to the SE (SD-3a) (Fig. 5e), i.e. to the same direction as adjacent Permian strata. This boundary cuts the internal structure of the Permian strata, so it may be slightly oblique and steeper. The topographic surface of the basement exposed close to the NW parallels the plane that defines the Permian-basement boundary (SD-3a). The Permian series and its northwestern boundary are unconformably covered by lowermost Triassic strata (RP-20; Fig. 4). These observations collectively suggest that the northwestern boundary of the Permian strata is a SE-dipping and NE-SW trending nonconformity formed in Permian times, which is eroded away from the basement rocks located to the NW.

4.2.2. Alpine syn-orogenic faults and folds

Most Alpine structures are easily recognizable as they are exclusive to Cenozoic rocks. However, these structures are expected to affect the whole pre-Cenozoic record, including the Variscan basement. Structures meeting these characteristics comprise strike-slip faults, thrusts and folds.

Alpine strike-slip faults trend between NW-SE, N-S and NE-SW (Fig. 4). N—S— to NW-SE-trending faults are right-lateral, while N—S— to NE-SW-trending faults are mostly left-lateral. The strike of the reverse faults is dominantly NE-SW, showing a great majority of them an apparent tectonic transport towards the S-SE. The reverse fault dips are moderate to high, as inferred from mapping, but from this point onwards, all these fractures will be referred to as thrusts. Some thrusts show opposite tectonic transports and have been considered as back-thrusts. There are exceptions regarding the aforementioned dominant orientation of thrust planes. Two of them, with E-W strike, occur SE of Robledo de Corpes (RP-21; Fig. 4) and S of Pálmaces de Jadraque (RP-20 and 22; Fig. 4). NE of Riofrío del Llano, there is also a NW-SE-trending thrust (RP-23; Fig. 4). Thrusts and normal faults have dip directions to the NW (RP-24, 25 and 26; Fig. 4).

The Cercadillo thrust (see location in Fig. 8a) is S-dipping and affects Mesozoic strata. The fault zone of this thrust is well exposed (Figs. 8b and c) and was analyzed by means of stress inversion applied to a fault population of 7 fault-slickensides couples. Slickenline pitches are close to 90°, σ1 is horizontal and trending N-S, while σ_3 is vertical (Shape factor $R = (\sigma1 - \sigma2) / (\sigma1 - \sigma3) = 0.67$, with 0.2 friction angle and a low misfit = 5–15) (Fig. 8d). These results are consistent with dominant N-S Alpine compression. However, the regional tectonic transport is to the S, so this fault would represent a backthrust.

Strike-slip and dip-slip faults do not intersect each other but merge and/or join to one another (RP-27 and 28; Fig. 4). Dip-slip faults tend to strike at right angles to the strike of strike-slip faults. Strike-slip faults are located at the hanging wall to dip-slip faults. Collectively, the strike-slip faults meet the criteria to be considered as tear faults, most, if not all of the dip-slip faults being coeval to them (Alpine) in a broad sense.

The thrusts in the study area are spatially related to folds that affect both the metamorphic basement and its Mesozoic and Cenozoic sedimentary cover (except Late Miocene to Pliocene sediments). In the case of the cover, the best examples are in the southern part of the study area (Fig. 6g). The southernmost thrust exposed in the study area cuts Cretaceous strata and juxtaposes them against Cenozoic strata (RP-22; Fig. 4). Close to this thrust there is a footwall synform cored by Cenozoic strata to the S (RP-29; Fig. 4) and a hanging wall antiform to the N (RP-30; Fig. 4). This antiform hosts at its core a set of N-dipping imbricate thrusts, which collectively cut at a moderate angle the S-dipping backlimb defined by Mesozoic strata (Fig. 5e). Equivalent structural relationships are observed along the eastern continuation of this thrust front (RP-31; Fig. 4). Fault imbrications are not exclusive to the sedimentary cover since they are also observed in thrusts that affect basement rocks (RP-7 and 8; Fig. 4). Overall, the fold-thrust relationships

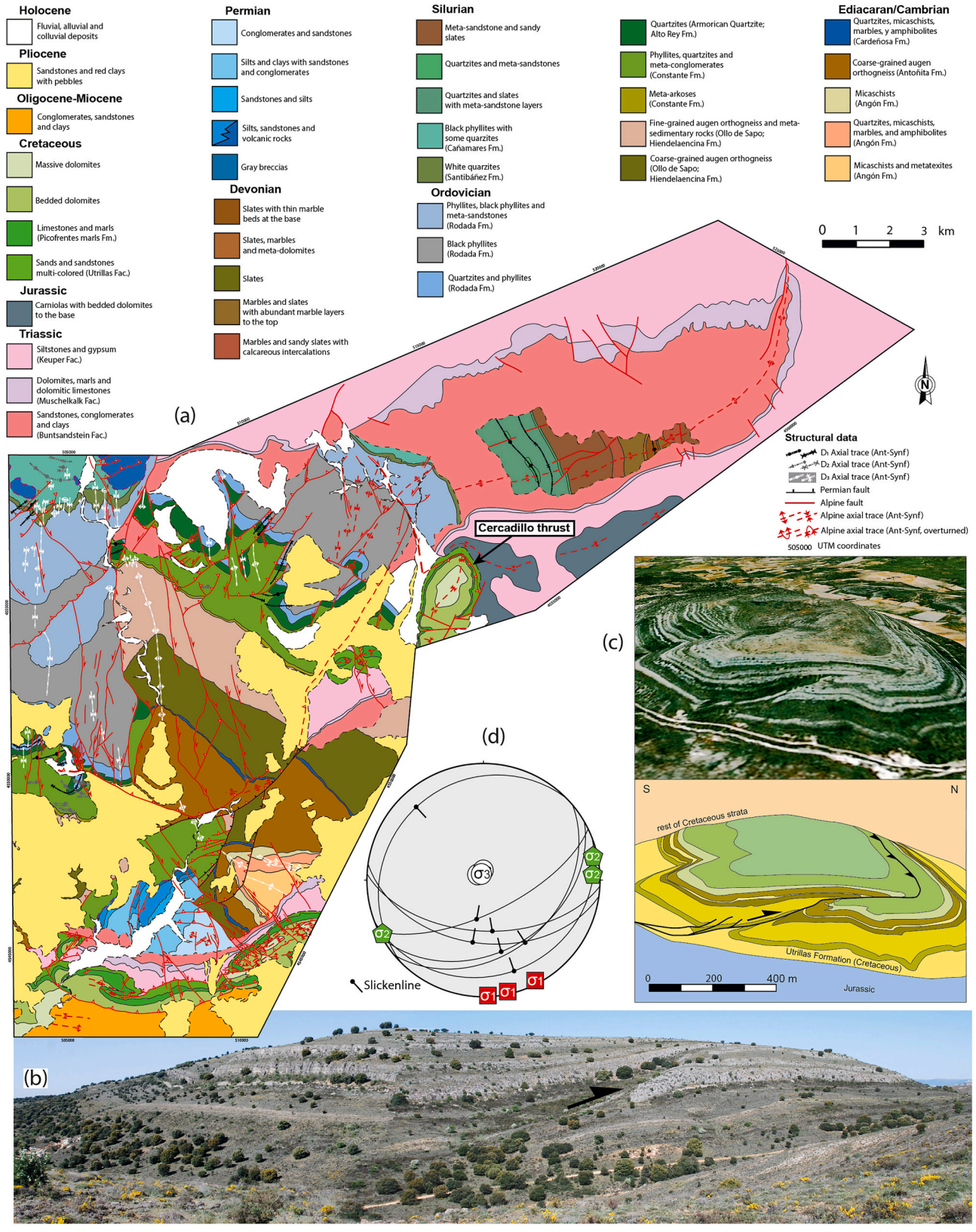

Fig. 8. (a) Map of the study area enlarged towards NE. Cartographic data for the enlarged area obtained from Ardell Argilés et al. (1982). (b) Panoramic view of the Cercadillo thrust observed from the E (see location in section a). (c) Structural and stratigraphic synthesis of a 3D panoramic view of the Cercadillo thrust observed from the E. (d) Stress inversion method applied to a fault population of 7 fault-slickensides and slickenlines couples. σ_1 is horizontal and trends roughly N-S, whereas σ_3 is vertical.

suggest that these are fault-propagation folds and that probably most reverse faults of the study area are part of a complex Alpine imbricate structure that involves the basement.

The structure of the Mesozoic cover reveals more Alpine folds, yet in sectors dominated by metamorphic basement rocks. Especially relevant is the antiform defined by NW-dipping Triassic strata near Naharros (RP-32 and 33; Fig. 4) and NE-dipping strata near Riofrío del Llano (RP-34; Fig. 4). The closure of this fold (and parasitic folds related to it) is defined by S_0 and S_1 in basement rocks at its core (RP-35; Fig. 4) (Fig. 6h), but it is traced by the basal contact of the Triassic series NE of the study area (Fig. 8a). This antiform is located in the hanging wall to a SE-directed thrust that connects two dextral strike-slip faults. Its axial trace runs NE-SW from the N of the Pálmaces de Jadraque dam (RP-36; Fig. 4), passing through the W of Cardeñosa (RP-24; Fig. 4) and up to N of Riofrío del Llano (RP-37; Fig. 4). This antiform seems equivalent to others defined by S_2 in basement rocks located along the hanging wall of its underlying thrust (RP-38; Fig. 4), and is paired with the underlying footwall synform defined by Mesozoic strata (RP-39; Fig. 4). The antiform is slightly asymmetric and SE-verging, as inferred from the folded structure of basement rocks that define a longer backlimb to the NW (between RP-33 and RP-35; Fig. 4) and a shorter forelimb to the SE (between RP-35 and RP-34; Fig. 4). The vergence of this fold fits well with the tectonic transport of its underlying thrust, as expected for fault-propagation folds. In the metamorphic (phyllitic) core of this antiform, there exist kink folds and kink bands affecting the regular layering defined by $S_0 + S_1$ in phyllites (SD-6f). Fold axial planes are parallel to kink bands and to a local fracture cleavage, both oriented 077°/70°. The orientation of the fold axes of these kinks is 35°/005°, and together with their axial planes they roughly parallel the regional axial plane and fold axis calculated for this major antiform from individual measurements of S_0 and S_1 (Fig. 6h). Those orientations do not correspond to any other local structures but D_1 folds. Since these kinks affect S_1, the kinks are considered Alpine in age, like in other areas of the Spanish-Portuguese Central System (de Vicente et al., 2021).

The southern limb of another Alpine fold is defined by S-dipping Triassic strata located to the S of the Pálmaces de Jadraque reservoir (RP-40; Fig. 4) and its eastern continuation up to Angón (RP-41; Fig. 4). The northern limb occurs close to Cardeñosa (RP-42; Fig. 4). The axial trace of the resulting antiform changes its trend from NE-SW-trending in the eastern part to E-W- and even ESE-WNW-trending in the western part. The core of this antiform consists of metamorphic basement rocks. These rocks are locally affected by kink folds analogous to those described before (SD-6f), although in this case kink folds are upright and trend NE-SW (RP-15; Fig. 4), i.e. parallel to the local axial trace of the major fold defined by Triassic strata. Also, in the core of this antiform, but to the W, the Permian strata is bent and define an open, WNW-ESE-trending antiform (RP-43; Fig. 4), slightly oblique to the E-W-trending antiform defined by Triassic strata due to the primary obliquity between Permian and (unconformable) Triassic strata (RP-40; Fig. 4). For the same reason, the primary obliquity between basement rocks and overlying cover (RP-33 and 42; Fig. 4) may preclude mappable Alpine folds to be formed and observed in basement rocks.

The bulk of the metamorphic basement, from N of Naharros (RP-32 and 33; Fig. 4) to the S between Pálmaces de Jadraque (RP-20 and 40; Fig. 4) and Angón (RP-41; Fig. 4), occupies the core of at least one (regional-scale) Alpine antiform (note dip direction of Triassic strata). This fold may actually be the same one whose closure is observed in the NE sector, both defined by metamorphic rocks (RP-35; Fig. 4) and Mesozoic strata (Fig. 8a).

5. Discussion

5.1. Early Variscan orogenic building

The D_1 structural record implies that early Variscan deformation led to crustal thickening (Soers, 1972; González Lodeiro, 1980; Fernández Rodríguez, 1991). The widespread nature of S_1 (including relicts) suggests that D_1 affected the entire basement. D_1 formed under low temperature conditions in the upper part of the regional structure (chlorite-biotite zone). In the lower part, kyanite porphyroblasts lack of internal fabric (SD-4 l), as opposed to staurolite and garnet (SD-4c, d, e and m). The latter grew during D_2, once S_1 was formed, while kyanite, despite lacking of S_1 microinclusions, could have formed during prograde metamorphism in the transition between D_1 to D_2. D_2 is related to crustal thinning (see discussion below). If so, the metamorphic assemblages related to D_2 decompression (garnet-staurolite-kyanite, and eventually sillimanite in some gneisses) suggest that D_1 thickening was a crustal scale process with at least moderate P/T gradient.

Early Variscan thickening in the Central Iberian Zone is acknowledged as a composite process. Part of the thickening is explained by the overriding of parautochthonous and allochthonous terranes (Rubio Pascual et al., 2016). We have not found any direct structural evidence of this in the study area (e.g., early Variscan thrusts). The rest of the thickening is fulfilled by E-verging overturned folds (such as those of the study area), which are dated at Carboniferous (354–347 Ma; Rubio Pascual et al., 2013) and account for the foreland-ward propagation of a growing collisional orogen that started in the Early Devonian (Dallmeyer et al., 1997; Díez Fernández et al., 2016).

5.2. Syn-orogenic Variscan extension

D_2 structures collectively define a regional shear zone with top-to-the-SE kinematics, as typified by: the heterogeneous distribution and penetrativeness of S_2, the development of asymmetric structures with consistent shear sense indicators, the rotation of pre-D_2 structures towards the same reference plane, the orientation of D_2 mineral and stretching lineations, and the increase of regional strain towards the same structural domain. This shear zone was referred to as the Hiendelaencina shear zone (González Lodeiro, 1980; Fernández Rodríguez, 1991), for which we will discuss the boundaries, conditions of formation, kinematics, primary geometry and age.

At the macroscale, D_2 structures collectively define an upper domain less penetratively affected by D_2 structures (S_1 remains the main foliation), and a lower domain strongly reworked by S_2 (S_1 is relict, if present). A quantitative approach to the distribution of regional deformation indicates that the lower structural levels of the region accumulate more strain, and that the strain is heterogeneously distributed and higher near lithological boundaries (Rf/φ and Fry methods; Fernández Rodríguez, 1991). The sections accumulating more strain match the sections dominated by S_2, i.e. strain is notably higher from the top of the Ollo de Sapo Formation downwards (as evidenced by the spatial distribution of finite deformation ellipsoids in Fernández Rodríguez, 1991 and Martínez Catalán et al., 2004). The geometry of meso- and macrostructures also suggests that D_2 tangential deformation increases downwards from the top of the Ollo de Sapo Formation. Above that structural level, D_2 macrofolds are either symmetric (RP-13; Fig. 4) or result from deflection of previous structures (i.e., equivalent to drag folds, RP-2; Fig. 4). Structurally downwards but still above the Ollo de Sapo Formation, D_2 folds become markedly asymmetric but with backlimbs bearing stratigraphic series in normal position (RP-11 and 12; Fig. 4) (SD-5f). D_2 folds are also asymmetric within the section dominated by S_2, but backlimbs fall within more strained domains and suggest fold asymmetry is reversed (SD-5e). The distribution of D_2 asymmetric microstructures point to the same increase of tangential deformation, because such structures are always present alongside S_2 in the lower structural levels, but S_2 does not always include them in the upper structural levels. Overall, we place the upper boundary of the Hiendelaencina shear zone atop the Ollo de Sapo Formation, the whole lower section of the metamorphic basement of the study area being the shear zone itself. The lower boundary of the shear zone is unexposed, so a minimum thickness of ~7 km is estimated for the shear zone.

Deformation conditions vary across the Hiendelaencina shear zone.

The shear zone *s.s.* formed under amphibolite facies metamorphic conditions (S_2), including garnet, staurolite, kyanite, and sillimanite. D_2 metamorphism within the shear zone was prograde. First, S_2-garnet includes crenulated S_1 whereas S_2-staurolite does not contain S_1 alone but also S_2, indicating a later growth of staurolite during D_2. And second, kyanite-bearing rocks occur alongside sillimanite-bearing rocks. The hanging wall to the shear zone did not remain unstrained during D_2, as it was deformed under greenschist facies metamorphic conditions. The development of S_2 mineral assemblages, typical of the biotite-chlorite zone, plus the development of low-dipping D_2 faults and tension gashes that even cut across S_2 (SD-3f), suggest a cooling path and eventual brittle-plastic deformation conditions in the hanging wall during D_2. However, the growth of large *syn*-D_2 biotite porphyroblasts in the (cold) hanging wall (phyllites) to the Hiendelaencina shear zone reminds of a thermal, and therefore ephemeral and prograde metamorphism (SD-4j and k). In the absence of heat sources such as plutons, this type of metamorphism can alternatively result from juxtaposition of a colder portion of crust (greenschist facies hanging wall) against a warmer one (amphibolite facies shear zone), thus favoring moderate heat transfer upwards to the hanging wall (Álvarez-Valero et al., 2014; Díez Fernández and Pereira, 2016). Yet, Fernández Rodríguez (1991) documented a widespread, post-D_2 recrystallization process (annealing) related to a heat source that also affected the rocks within the Hiendelaencina shear zone, particularly intense in the Angón Formation (the structurally lowest one exposed). This would suggest that the location of the main heat source would be unexposed and underlying the basement. Given the thermal conditions required to form S_2, the underlying heat source is very likely to be migmatitic and/or granitic in nature, as suggested by drill cores extracted nearby (Querol, 1989).

S_2 asymmetric microstructures suggest top-to-the-SE to -SSE kinematics for the Hiendelaencina shear zone. This sense of shear is compatible with the NW-wards rotation (drag) of D_1 fold axial traces near the upper boundary of the shear zone (RP-2, 6 and 7; Fig. 4). D_2 mineral and stretching lineations show variability in their orientation (Fig. 7b), which matches that of D_3 fold axes (Fig. 7c), to which those lineations may be partly reoriented (Fig. 6b). D_2 normal faults in the hanging wall to the Hiendelaencina shear zone show top-to-the-E (Fig. 7a) and -SE (SD-3e and SD-5b) kinematics, which indicates actual dispersion of D_2 tectonic flow that cannot be accounted for D_3 reorientation.

If measured normal to S_2, the distance between D_1 fold troughs and the upper boundary of the Hiendelaencina shear zone does not really change from E (RP-12; Fig. 4) to W (RP-11; Fig. 4), which suggests a primary flat-lying geometry for this section of the D_2 shear zone. Such a distance, easily traceable from the top of the Ollo de Sapo Fm. to the base of the Alto Rey Fm., does not really change several tens of km more to the W (González Lodeiro, 1980; Fernández Rodríguez, 1991). Given the top-to-the-SE kinematics of this shear zone, we envisage this section of the Hiendelaencina shear zone either as a long flat of a larger D_2 megastructure or as representative of the overall flat-lying geometry of the entire megastructure.

The Hiendelaencina shear zone was recognized as a ductile thrust in previous studies (González Lodeiro, 1980; Fernández Rodríguez, 1991; Martínez Catalán et al., 2004). However, there is no observable large-scale (asymmetric) duplication (expected for a thrust), except for local D_2 mesoscale folds (e.g., RP-13; Fig. 4). In any case, this type of folds, even with recumbent geometry and able to duplicate (symmetrically) the series, is not direct evidence of net crustal thickening, as they can be formed in extension-dominated settings (Froitzheim, 1992; Harris et al., 2002) and have been found to accommodate vertical shortening in ductile extensional shear zones of the Central Iberian Zone (Arango et al., 2013; Díez Fernández et al., 2013, 2017, 2019a, 2019b). If analyzed at a large scale, all of the pre-Variscan series are in normal position (Fig. 4), so the duplication of this piece of orogenic crust by D_2 structures is not supported by data.

The tectonothermal record (M_1) prior to the development of the Hiendelaencina shear zone defines a normal gradient, and so does the record (M_2) related to the shear zone itself. Measured normal to S_2, the distance between the hotter sections (sillimanite-bearing) and rocks deformed during D_2 within the biotite-chlorite zone is approximately 7 km (roughly 2 kbar in lithostatic P), maybe less if Alpine thrusting is restored. The resulting thermal gradient does not seem to correspond to a thickened but to a thinned crust. Crustal thinning likely applies to the M_1 record too, since kyanite-bearing rocks occur few hundred meters far across S_2 planes from sections affected by low-grade M_1 metamorphism (biotite-chlorite zone). The thinning of the M_1 thermal structure and the higher-T gradient during M_2 can be attributed to the Hiendelaencina shear zone, which emerges as an extensional shear zone. Such character is also supported by the set of brittle-ductile D_2 extensional structures of its hanging wall (SD-5b and 6e, RP- 9; Fig. 4) and by the development of near-vertical tension gashes (SD-3f). To the West of the study area, $^{40}Ar/^{39}Ar$ dating of S_2 fabrics related to *SE*-directed extensional flow yielded an age range of 335–327 Ma (Rubio Pascual et al., 2013), which fits with the range obtained from U—Pb dating of M_2 monazite (Valverde Vaquero et al., 1996). We consider the Hiendelaencina shear zone to be formed within that age range.

The primary flat-lying geometry inferred for the (top-to-the-SE) Hiendelaencina shear zone suggest that if this shear zone was extensional and not purely flat, it would have very shallow dipping to the SE. D_2 tension gashes have been used to calculate the orientation of D_2 principal stresses (Fig. 7a). σ_1 is steeply plunging. Restoring the D_3 fold axis plunge (Fig. 7b) to the horizontal would take σ_1 to a primary subvertical orientation, which is key to produce extensional faults. Another evidence of the extensional nature of the Hiendelaencina shear zone is the spatial distribution of the finite strain, the magnitude of which increases towards the SE, that is, towards the frontal part of the structure (Fernández Rodríguez, 1991; Martínez Catalán et al., 2004). This distribution is contrary to that expected for a push-from-the-rear thrust sheet, although it is similar to that predicted for structures due to gravity spreading (e.g., Merle, 1998).

We think rheology plays a fundamental role in the location of the Hiendelaencina shear zone. The hanging wall is made of bedded and foliated metasedimentary rocks, whereas the shear zone mostly consists of foliated metaigneous rocks. Grain size in the hanging wall (mostly metapelitic phyllites) is notably smaller than in the shear zone (fine- to medium-grained augen orthogneisses). The hanging wall constitutes a low yield strength layer at the regional scale because of its greater content in phyllosilicate-rich rocks. This type of rocks is weaker than rocks bearing larger content in quartz and feldspar (Carter et al., 1964; Borg and Handin, 1966; Gottschalk et al., 1990), such as orthogneisses, and favors a decrease in strength and an increase in ductility with increasing mica content (Shea and Kronenberg, 1992, 1993). The primary bedded structure of the hanging wall metasedimentary rocks adds to their weaker rheology than the orthogneisses of the shear zone, which presumably had phaneritic and some porphyritic igneous textures. Overall, the contrasted rheology between the upper and weaker metasedimentary series and the lower and stronger orthogneissic section controlled the location of the upper boundary of the Hiendelaencina shear zone. Most of D_2 shearing did not concentrate within the apparently weaker domain, so the primary nature of the series is just another component controlling D_2 deformation. Temperature is a fundamental factor that affects the rheological behavior of rocks, making them less viscous (weaker) as it increases. Temperatures related to M_2 increase down structure, so the core of the Hiendelaencina shear zone hosted warmer and weaker rocks by comparison with its hanging wall. We propose a mixed rheological control model, in which the location of the shear zone was controlled by the regional thermal structure and its upper boundary by the primary rheological contrast between the rocks it affected. Contrasted initial composition (sedimentary versus igneous) and structure (bedded versus granular and homogeneous) acted together as a primary factor in controlling the upper boundary of the shear zone. Downward increasing temperature contributed to weaken

the piece of crust under that upper boundary, favoring metamorphic recrystallization (widespread development of S_2) and broad reworking of the infrastructure.

5.3. Late Variscan orogenic building

D_3 folds imply a second stage of Variscan crustal thickening under low temperature metamorphic conditions (sericite-chlorite-biotite zone). However, S_3 occurs both in sections that experienced low temperature and sections with high temperature metamorphism during D_2, so a global path of cooling existed from D_2 to D_3. D_3 regional shortening occurred in a similar (E-W) direction to D_1, favoring type-3 fold interference patterns (Ramsay, 1967) (PR-1; Fig. 4). The asymmetry of major D_3 folds suggests vergence to the W (PR-14 and 16; Fig. 4). In the Variscan Orogen, D_3 folds like these are coeval to strike-slip shear zones dated at 316–295 Ma (Rubio Pascual et al., 2013; Gutiérrez-Alonso et al., 2015; Díez Fernández and Pereira, 2017).

D_3 folds (axial planes and fold axes) trend asymptotically into an Alpine, N-S trending fault (PR-44-45; Fig. 4) that juxtaposes the backlimb and forelimb of the D_3 asymmetric structure of the region (Fig. 9). The curvature of the trend suggests D_3 dextral shearing, which would have formed a local strike-slip shear zone in a transpressional setting. D_2 lineations in that area show a similar asymptotic trend (Figs. 4 and 6b) that cannot be accounted for pure mechanical reorientation by the D_3

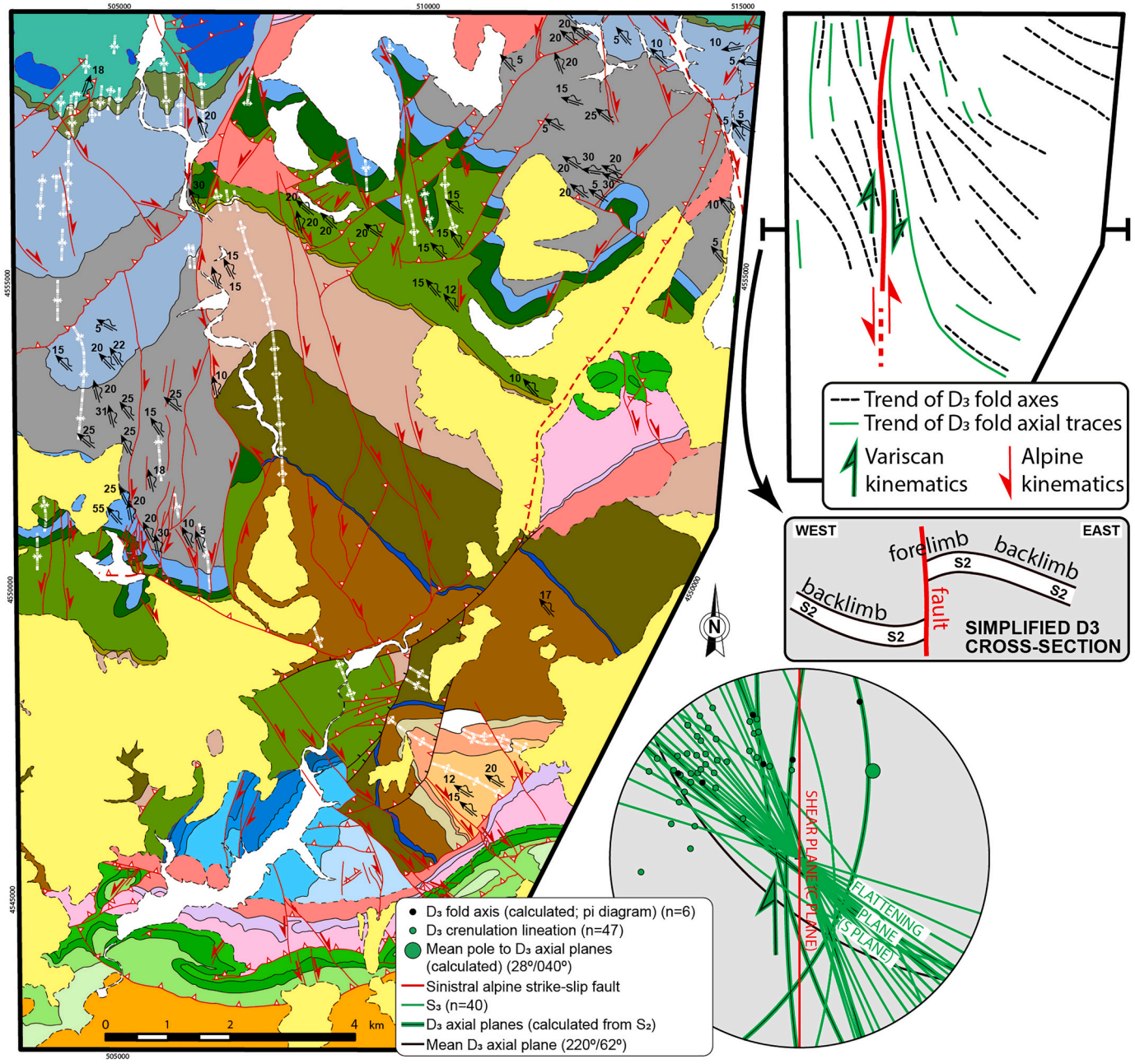

Fig. 9. Asymptotic and fan structure of D_3 fold axes and axial traces with respect to the sinistral Alpine strike-slip fault trace that appears in the western sector of the study area. The asymptotic structure is best observed in a geological map (left) and in a simplified map (right top) showing the orientations of D_3 fold axes and axial traces, which are included alongside a stereographic plot with all those structural data (S_3 axial planes, D_3 fold axes, and Alpine fault trace). Note the clockwise obliquity of the fault trace measured from S_3, which equals to or is less than 45°. The asymmetric, W-verging structure of major D_3 folds is summarized in a simplified cross-section.

upright antiform. Accordingly, the local deflection of D_2 linear fabrics adds to the evidence of a dextral shear zone. Major D_3 fold asymmetry is compatible with an upthrown movement of the eastern side of the shear zone. This potential throw would not have been compensated by the throw of the Alpine fault we see today. Moreover, that throw was likely enlarged during Permian tectonics (see below).

The Variscan Orogen experienced alternating stages of crustal thickening and thinning (e.g., Díez Fernández et al., 2013), D_3 reflecting the last pulse of orogenic building in the study area. The Gondwana-Laurussia convergence remained until the earliest Permian (Heredia et al., 2022), and except for the oroclinal folding that affected the entire orogen (Pastor-Galán, 2022), which may be coeval to D_3 (Martínez Catalán, 2011; Gutiérrez-Alonso et al., 2015), there is no evidence of post-D_3 Variscan deformation in the study area. However, in other sections of the orogen and within the Central Iberian Zone, D_3 is followed by extension driven by moderate- to high-dipping normal faults (Barbero, 1995; Capote et al., 2000; Arango et al., 2013; Rubio Pascual et al., 2013). None of this type of faults is directly observed in the study area, although they may have been reactivated and therefore blurred by younger tectonics (see below).

5.4. Post-orogenic Permian extension

The fractures that show normal fault offset are exclusive to Paleozoic rocks. Among the numerous fractures identified in the study area, we focus on those that were or could have been active during the Permian. The unconformable base of the Permian series is exposed (RP-19; Fig. 4). The Permian series define a progressive angular unconformity that wedges to that exposure (Sopeña, 1979). The eastern limit of the Permian series is a set of Alpine dextral strike-slip faults (referred to as Sarteneja fault; Sopeña, 1979; Fernández Rodríguez, 1991), whose associated (and limited) offset in Mesozoic strata can be explained by almost pure slip along strike. A qualitative restoration of their along-strike movement results in the Permian series located in a downthrown side of pre-Mesozoic near-vertical faults. These sub-vertical faults abruptly terminate the nonconformity at the base of the Permian series and the normal faults at their NE side (RP- 25-26; Fig. 4), which strike perpendicular to the subvertical faults and show the structure of an extensional transfer fault system. Given the likely synchrony between the sedimentation of the Permian series, the normal faults (see discussion below), and the sub-vertical faults, we propose a Permian age for the transfer fault system.

The northern horse associated with the Alpine, N-S trending sinistral strike-slip fault (RP- 44; Fig. 4) hosts the base of the Triassic series. The offset of that base with respect to its exposure outside the directional horse, to the E, suggests an upthrown movement of the western side of the strike-slip fault. The absence of Triassic strata to the W of this horse, or even further to the S along the trace of the fault, suggests that this (oblique?-) dip-slip movement probably occurred along the entire strike-slip fault during the Alpine Orogeny. If so, the relative downthrown movement of the western side of this fault, needed to explain the absence of Permian rocks (volcanic, volcanosedimentary and sedimentary) in the eastern side (see also Bascones Alvira et al., 1982), indicates that this fault functioned as a dip-slip normal fault during the Permian. The trace of this fault matches that of a Variscan D_3, strike-slip shear zone (Fig. 9), which we think provided a weak rheological domain to nucleate from and rework (or reactivate?) a former near-vertical structure.

Several Alpine thrusts are parallel to the normal faults that appear to the E of the Permian series (RP-25 and 26; Fig. 4). In the side that both types of fault share, there are N*E*-SW trending kinks compatible with Alpine subhorizontal shortening (RP-15; Fig. 4). These normal faults occur in a domain that was clearly subjected to Alpine contraction, as they are located at the core of an Alpine antiform (see fold limbs at RP-41 and RP-42; Fig. 4) and imbricate with Alpine thrusts. We suggest that these normal faults were inverted during Alpine contraction, only that the Alpine reverse slip was not enough to overcome the former, probably Permian, normal dip slip. This pair of normal faults strikes closer to a N-S trend than the rest of Alpine thrusts. Accordingly, the amount of Alpine reverse dip slip upon a hypothetic N-S contraction (see below) would be less for these faults, which retained their normal fault looking appearance inherited from Permian tectonics (Figs. 5b, c and f). The NW-SE vector of Permian extension is based on the dominant NE-SW trend of Permian normal faults. The strike-slip components of some Permian faults are speculative and based on the trend of individual faults relative to the main stretching direction inferred for the Permian period. This vector is compatible with that of the Berzosa Fault (Hernaiz Huerta et al., 1996), which is the main Permian extensional fault described in the region so far.

The partial inversion model also explains the geometry and local offset of the fault that imbricates with the pair of normal faults discussed above (RP-24, 36 and 37; Fig. 4). The reverse dip-slip of this fault is typified by the juxtaposition of Paleozoic metamorphic rocks against Mesozoic strata (RP-39; Fig. 4) and of structurally lower onto upper rocks of the metamorphic basement (RP-36; Fig. 4). The normal dip-slip of this fault is observed in a section where the orientation of the fracture changes from ENE-WSW to NE-SW (RP-24; Fig. 4), thus having a less favorable strike to accommodate N-S Alpine shortening via dip slip. In this section, Alpine shortening is also taken by other local structures such as minor thrusts and folds (RP-38; Fig. 4), which would have contributed to a lesser dip slip in other fault sections nearby.

Permian tectonics in the Iberian Massif is framed either into a late orogenic collapse (e.g., Lloret et al., 2021) or into a post-Variscan transtensional stage before the break-up of Pangea (Lago et al., 2004), which came along the development of sedimentary basins and magmatism (Sopeña et al., 1988; García-Lasanta et al., 2015). In the study area, this evolution is recorded in normal faults and strike-slip faults (reactivated during the Alpine Orogeny), sedimentary basins (Permian strata; Sopeña et al., 1988), and volcanic rocks (Atienza andesites; Schröeder, 1930). Permian normal faulting had already been put forward by Sopeña (1979) and Fernández Rodríguez (1990), but we propose more Permian faults and suggest (see below) that Permian faulting could have been a more pervasive process than previously considered. Moderate- to high-dipping normal faults cutting Variscan D_3 structures are recognized elsewhere in the Central Iberian Zone (Barbero, 1995; Capote et al., 2000; Arango et al., 2013; Rubio Pascual et al., 2013). Although they are classically framed into a late-Variscan setting (e.g., Hernaiz Huerta et al., 1996; López-Gómez et al., 2002; Rubio Pascual et al., 2013), their relative timing accords well with a broad period of extension that followed the Variscan Orogeny and heralded the break-up of Pangea. Given that none of those normal faults are coeval to a process of orogenesis elsewhere in the Variscan Orogen (i.e., mountain building) but to mountain dismantling and subsiding basins, we prefer to observe them out of an orogenic event and as part of a post-collisional, transient process before the onset of a new (Alpine) tectonic cycle (post-orogenic collapse; Lloret et al., 2021; Heredia et al., 2022).

5.5. Cenozoic shortening: Alpine Orogeny

The Cenozoic structural imprint includes tear faults, thrusts and associated folds that collectively account for deformation partitioning. The set of dextral and sinistral strike-slip faults is compatible with σ_1 being sub-horizontal and N-S trending, as proposed by de Vicente et al. (2018) for the Spanish-Portuguese Central System. The southern foreland of this Alpine mountain range is located to the south of the study area (Madrid Basin; Fig. 3). Towards this foreland, the Alpine thrusts trend roughly *E*-W and do not involve metamorphic basement (RP-20, 22, 30 and 31; Fig. 4), so they do not seem reactivated fractures. If so, the E-W Alpine thrusts support the same σ_1 cited before, as expected for the synchronous nature between Alpine strike-slip faults and reverse faults inferred from their geometrical relationships. Such set of Alpine faults is equivalent to the one observed in the Variscan basement of NW Iberia

(Martín-González and Heredia, 2011a, 2011b).

Most Alpine thrusts in the Paleozoic rocks trend NE-SW. This is compatible with N-S shortening, but these fractures do not conform to N-S trending σ_1 alone, which would have produced E-W trending thrusts. The study area experienced fracturing during the Permian. In fact, some NE-SW Alpine faults are parallel to Permian faults reactivated during Alpine contraction (see above). We suggest that the mismatch between the ideally expected and actually observed fault trend is due to structural inheritance from Permian extension, which sometimes is itself controlled by local inherited Variscan structures. Accordingly, some of the strike-slip faults that now connect Alpine thrusts could be Permian transfer faults that connected normal faults. The dip of the Alpine reverse faults in the study area is moderate to high, mostly greater than 45° and usually within the 60°-70° range, even for some cover areas. A

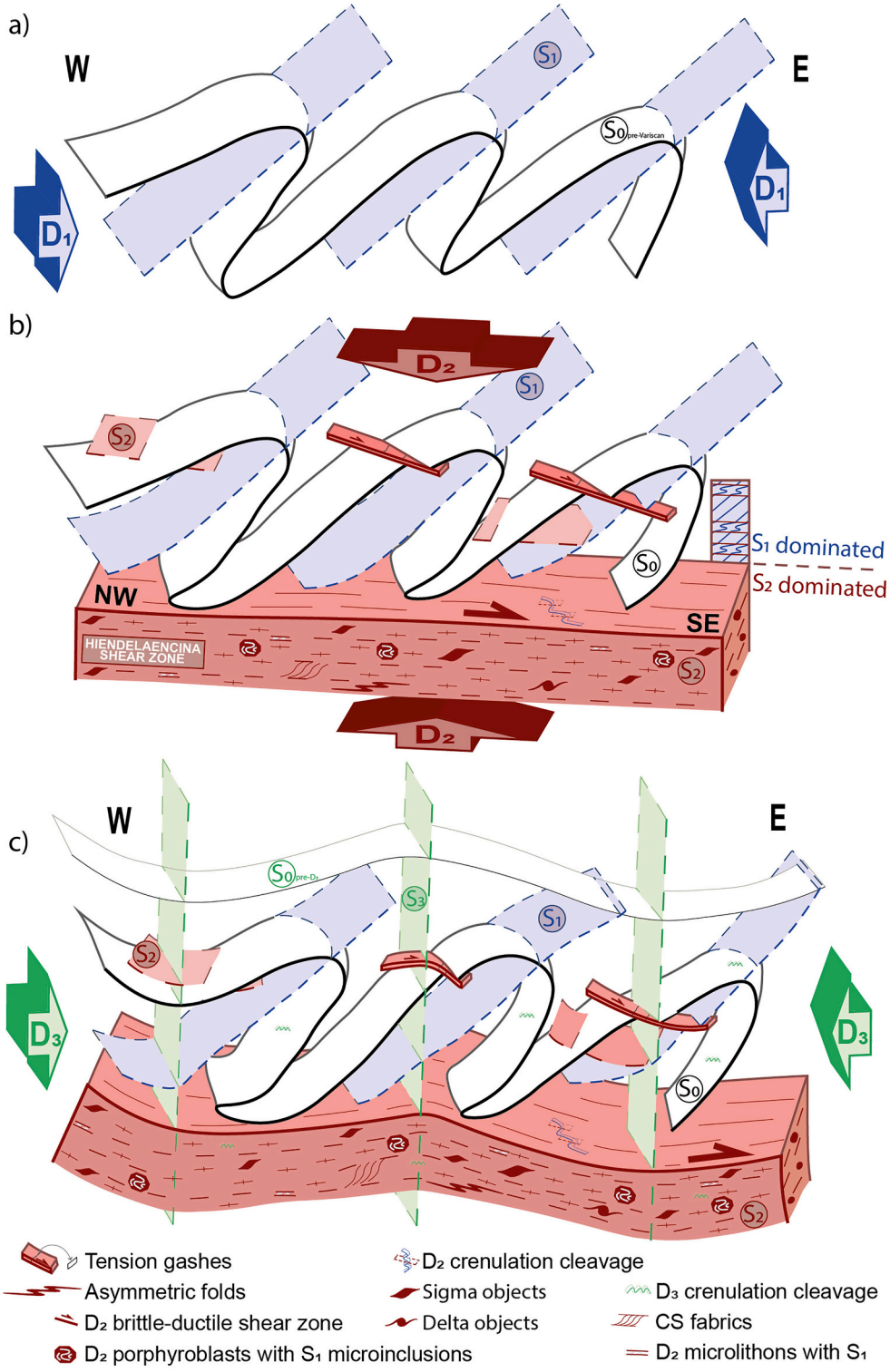

Fig. 10. Model of Variscan orogenic evolution for the study area. The model includes the main structures formed during each deformation phase: a) D_1, b) D_2 and c) D_3, as well as their interference.

good example of the latter is the Alpine thrust imbricate that runs from RP-30 to RP-31 (Fig. 4), which dips towards the opposite direction to the backlimb defined by Mesozoic strata at its hanging wall (Fig. 5e). We also propose such geometry and the imbricate structure of the thrusts as a likely inheritance from Permian normal faults.

Part of the Alpine strike-slip faults trends close to N-S, which is not expected for a conjugate fault system formed under horizontal, N-S trending σ_1. Yet, such maximum principal stress would allow for both right- and left-lateral slip along former planar anisotropies trending close to N-S. Fractures that moved during the Permian show this pattern (e.g., RP-45 and 46; Fig. 4), so others with similar geometry and Alpine kinematics could hold a Permian record too.

5.6. *The role of inheritance*

The tectonic evolution of the study area shows multiple examples of reworking and reactivation (sensu Holdsworth et al., 2001). The superposition of penetrative fabrics (S_1-S_2-S_3; Figs. 10 a, b and c respectively) takes place alongside metamorphism, which is exclusive to the Variscan Orogeny. This fabric superposition does not reflect a single protracted tectonic event, as typified by (i) the contrasted metamorphic conditions to form each fabric, (ii) the different absolute age for their

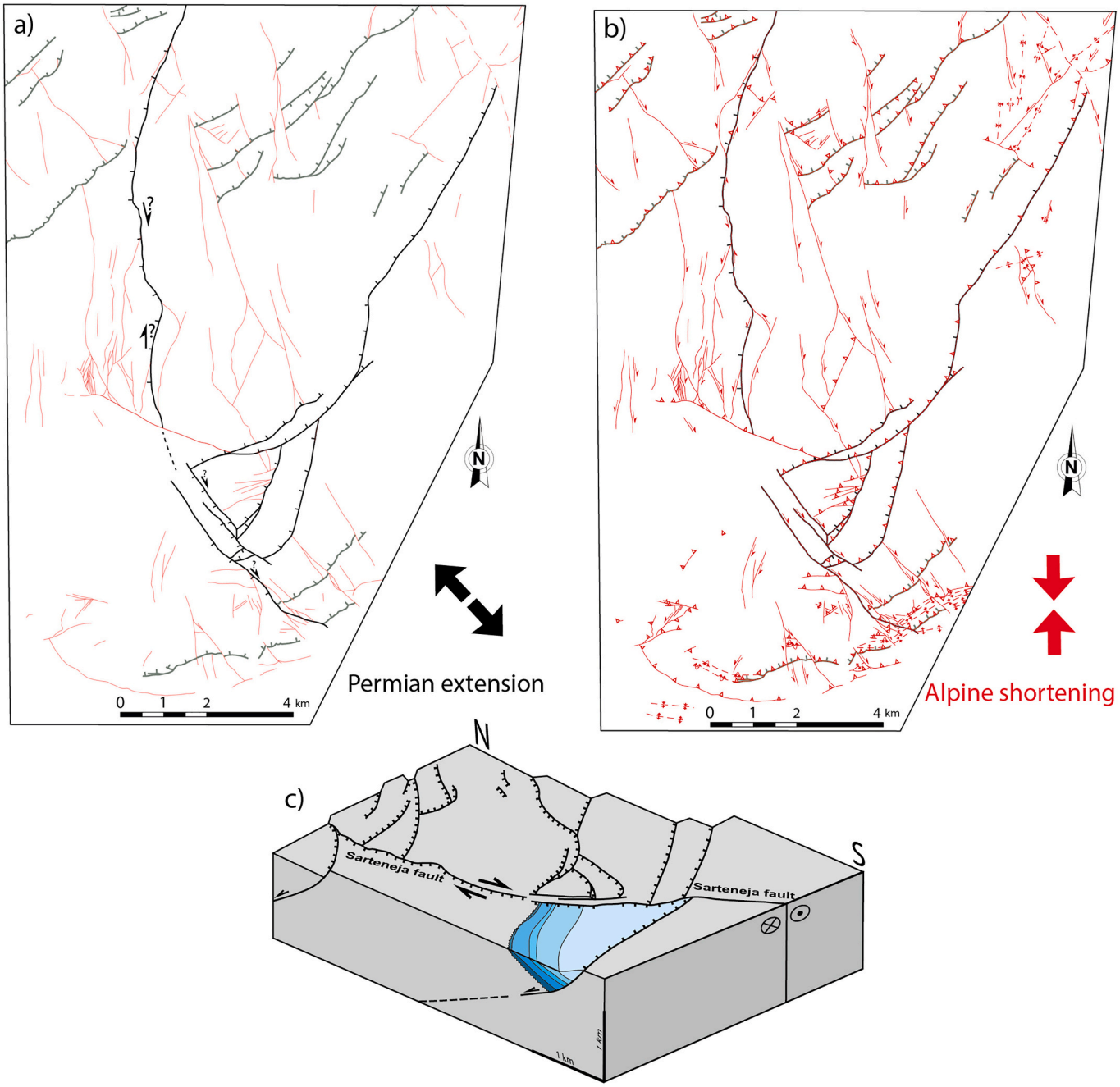

Fig. 11-. Map views showing simplified structural models of the (a) Permian extension and (b) Alpine shortening. The models highlight the inverted nature of normal faults and the reactivation of both strike-slip and normal faults upon superimposed contraction. Pale red colour in (a) refers to future Alpine faults, while pale grey is used for suspected Permian normal faults. The model for the Permian period is illustrated in 3D in section c, which intends to show the relationships between Permian sedimentation and graben development in the eastern side of the Sarteneja strike-slip fault in a context of extension. Blue colors in section c follow those of the Permian series in Fig. 4. (For interpretation of the references to colour in this figure legend, the reader is referred to the web version of this article.)

development (spanning a total of ~60 million years), and (iii) the contrasted stress field under which they were created. Accordingly, the interference between the set of Variscan structures that were grouped into different phases of deformation and have regional extent (D_1-D_2-D_3) represents reworking. Variscan reworking is produced in two different ways. In the one hand, the deformation of former structures by superimposed folds and/or shear zones occurs throughout most of the tectonic history. On the other hand, new fabric generation at the expense of previous ones is penetrative (e.g., S_1 is deeply blurred by S_2 down structure). Reactivation is a more complex issue in the study area. Although reactivation seems restricted to faults, there is evidence that penetrative planar anisotropies (such as S_0 and S_3) also played a role and controlled the structures that followed by providing a weak rheology to exploit (e.g., reactivation of the D_3 shear zone during Permian and Cenozoic deformation).

The earliest reactivation we propose for the study area relates to D_2. The upper boundary of the Hiendelaencina shear zone is controlled by the contrasted rheology between (softer) hanging wall and (harder) footwall (see discussion above). This would not represent a reactivation of a specific planar structure sensu stricto, but the reactivation of a virtual weak domain (tabular in shape) defined by the primary composition of pre-Variscan Paleozoic rocks. This domain (few meters thick) is diffuse but thin by comparison with the size and thickness of the hanging wall and footwall of the Hiendelaencina shear zone.

The location of the D_3 strike-slip shear zone in the study area does not seem to be controlled by previous anisotropies, but it influenced how deformation parted during the tectonic evolution that followed. Permian extension was in part conducted through the reactivation of this shear zone as a transfer fault (Fig. 11a). We think that the absence of D_3 strike-slip shear zones in other sections of the Iberian Massif could have favored Permian extension via moderate-dipping normal faults alone (e.g., Santa María de la Alameda Fault, Berzosa Fault, Toledo Fault; Barbero, 1995; Capote et al., 2000; Arango et al., 2013; Rubio Pascual et al., 2013). But if previous strike-slip shear zones existed, like in the study case, Permian extension was accommodated by slip along strike those (reactivated) Variscan shear zones and dip slip along (newly formed) normal faults. Interestingly, the throw of individual Permian normal faults increases in the absence of D_3 strike-slip shear zones, so we speculate that the partitioning effect during the Permian reactivation of D_3 strike-slip shear zones would have prevented normal dip-slip faults to be formed at crustal scale.

The orientation of Alpine structures that affects the Variscan basement of the study area is strongly conditioned by the previous structural record (Fig. 11b). In several cases there is evidence that Permian extension was not overcome by Alpine shortening, but the latter reactivated most of the largest Permian faults of the study area. The trend of the intraplate chain that defines the Spanish-Portuguese Central System is NE-SW, which is not orthogonal to the N-S compression inferred for its uplift (de Vicente et al., 2018). An important part of the Permian faults in the region trend parallel to that Alpine intraplate chain, so the Permian normal faults could have conditioned part of its geometry, just like in our study area. This hypothesis considers the eastern part of Spanish-Portuguese Central System as a mountain range that resulted from the inversion and reactivation of Permian extensional transfer fault systems. This idea acknowledges the fundamental role that pre-orogenic structural inheritance played during the uplift of the Spanish-Portuguese Central System, some of whose sections are also believed to be built after reactivation of Permian normal faults such as the Berzosa Fault (de Vicente et al., 2022).

Temperature seems the determining factor controlling whether reworking or reactivation occurs in the studied area throughout its deformational record. Variscan deformation in our study case is always accompanied by metamorphism, which could have prevented or lessened the chances for reactivation to occur. Upon a warm-enough orogenic crust, Variscan superimposed stress generated new structures that interfere and are not conditioned by the previous deformational history. The Permian and Alpine structures exposed today formed under cold conditions (no metamorphism), and in both cases reactivation is the rule.

6. Conclusions

The metamorphic basement of the eastern section of the Spanish-Portuguese Central System records deformation related to the building and dismantling of the Variscan Orogen, to the Permian extensional tectonics that heralded the break-up of Pangea, and to the building of an intraplate mountain range during the Alpine Orogeny. Structural inheritance and lithological composition throughout that tectonic history conditioned how either regional contraction or extension was taken by structures during subsequent deformation.

Early Variscan crustal thickening is attested by E-verging overturned folds and prograde metamorphism reflected in axial plane foliations (D_1). In a subsequent context of orogenic collapse, crustal attenuation was driven by a top-to-the-SE ductile, extensional shear zone (D_2) that produced heterogeneous reworking of the D_1 record. D_2 shearing favored intense reworking (recrystallization) of the rocks in the shear zone and moderate to gentle reworking at its hanging wall. The upper structural boundary of the D_2 shear zone is marked by a zone separating protolith rocks with contrasted rheology (sedimentary vs. igneous rocks), so the extent of D_2 reworking seems partly controlled by primary composition. Late Variscan crustal thickening was performed by a dextral, N-S trending strike-slip shear zone (D_3). D_3 produced gentle reworking of former structures by producing upright folding of the previous fabrics and axial plane foliation at both sides of the D_3 shear zone.

None of the Variscan structures exposed in the study area was reactivated during the Variscan Orogeny itself. However, the D_3 strike-slip shear zone influenced how deformation was accommodated thereon. Permian extension reactivated the D_3 shear zone as a normal and likely transfer fault, to which a seemingly high number of normal faults connected. Alpine contraction also reactivated this strike-slip shear zone as a sinistral fault. N-S Alpine contraction favored the inversion of most Permian faults while part of the basement was bent into hanging wall folds related to that inversion. In a setting of N-S Alpine contraction in Central Iberia, the anomalous structural trends of Alpine structures, such as N-S trending faults or NW-SE and NE-SW trending thrusts, can be explained through fault reactivation. This observation also applies to the regional NE-SW trend of the Spanish-Portuguese Central System, which may be a reflection of Permian structural inheritance. Anomalous structural trends in an orogen, according to regional stress, may be related to structural inheritance. Such anomalies can be used as a starting point to unveil a longer path of deformation for specific structures. At a larger scale, anomalously trending mountain ranges with respect to the principal stresses that raised them could be an indication of the paleo-trends of lithosphere necks lost to superimposed contraction.

Supplementary data to this article can be found online at https://doi.org/10.1016/j.tecto.2022.229601.

Data availability statement

Data are available through Moreno-Martín et al. (2021).

Declaration of Competing Interest

The authors declare the following financial interests/personal relationships which may be considered as potential competing interests.

Diana Moreno Martín reports financial support was provided by Ministerio de Ciencia, Innovación y Universidades MCIN/AEI/ 10.13039/501100011033. Rubén Díez Fernández reports financial support was provided by Ministerio de Ciencia, Innovación y Universidades MCIN/AEI/ 10.13039/501100011033. Diana Moreno Martín reports

financial support was provided by University of Salamanca MUGA21.

Data availability

Data are available through Moreno-Martín et al. (2021)

Acknowledgments

This publication is part of project PID2020-112489GB-C22, funded by MCIN/AEI/ 10.13039/501100011033. This work includes the MSc project of DMM partially funded by MUGA21-University of Salamanca. We would like to thank Daniel Pastor-Galán, Paul Angrand and one anonymous reviewer for their valuable comments.

References

Aldega, L., Viola, G., Casas-Sainz, A., Marcén, M., Román-Berdiel, T., van der Lelij, R., 2019. Unraveling multiple thermotectonic events accommodated by Crustal-Scale Faults in Northern Iberia, Spain: insights from K-Ar Dating of Clay Gouges. Tectonics 38 (10), 3629–3651.

Álvarez-Valero, A.M., Gómez Barreiro, J., Alampi, A., Castiñeiras, P., Martínez Catalán, J.R., 2014. Local isobaric heating above an extensional detachment in the middle crust of a Variscan allochthonous terrane (Órdenes complex, NW Spain). Lithosphere 6 (6), 409–418.

Andrés, J., Draganov, D., Schimmel, M., Ayarza, P., Palomeras, I., Ruiz, M., Carbonell, R., 2019. Lithospheric image of the Central Iberian Zone (Iberian Massif) using global-phase seismic interferometry. Solid Earth 10, 1937–1950.

Andrés, J.M., Ayarza, P., Schimmel, M., Palomeras, I., Ruiz, M., Carbonell, R., 2020. What can seismic noise tell us about the Alpine reactivation of the Iberian Massif? An example in the Iberian Central System. Solid Earth 11, 2499–2513.

Angelier, J., 1979. Determination of the mean principal directions of stresses for a given fault population. Tectonophysics 56, T17–T26.

Angrand, P., Mouthereau, F., 2021. Evolution of the Alpine orogenic belts in the Western Mediterranean region as resolved by the kinematics of the Europe-Africa diffuse plate boundary. BSGF-Earth Sci. Bull. 192 (1), 1–44.

Angrand, P., Mouthereau, F., Masini, E., Asti, R., 2020. A reconstruction of Iberia accounting for Western Tethys-North Atlantic kinematics since the late-Permian-Triassic. Solid Earth 11 (4), 1313–1332.

Arango, C., Díez Fernández, R., Arenas, R., 2013. Large-scale flat-lying isoclinal folding in extending lithosphere: Santa María de la Alameda dome (Central Iberian Massif, Spain). Lithosphere 5, 483–500.

Ardell Argilés, F., González Lodeiro, F., Tena-Dávila Ruiz, M., 1982. Mapa geológico de la Hoja n° 434 (Barahona). Mapa Geológico de España 1:50.000. Segunda Serie (MAGNA), Primera edición. IGME.

Azor, A., Dias Silva, Í., Gómez Barreiro, J., González-Clavijo, E., Martínez Catalán, J.R., Simancas, J.F., Martínez Poyatos, D., Pérez-Cáceres, I., González Lodeiro, F., Expósito, I., Casas, J.M., Clariana, P., García-Sansegundo, J., Margalef, A., 2019. Deformation and structure. In: The Geology of Iberia: A Geodynamic Approach. Springer, Cham, pp. 307–348.

Barbero, L., 1995. Granulite-facies metamorphism in the Anatectic complex of Toledo, Spain: late Hercynian tectonic evolution by crustal extension. J. Geol. Soc. 152 (2), 365–382.

Bascones Alvira, L., González Lodeiro, F., Martínez Alvarez, F., Gabaldón López, V., Ruiz Reig, P., 1982. Mapa geológico y Memoria de la Hoja n° 433 (Atienza). Mapa Geológico de España E. 1:200.000 ITGE, p. 47.

Baud, P., Louis, L., David, C., Rawling, G.C., Wong, T.-F., Bruhn, D., Burlini, L., 2005. Effects of bedding and foliation on mechanical anisotropy, damage evolution and failure mode. Geol. Soc. Lond. Spec. Publ. 245 https://doi.org/10.1144/GSL.SP.2005.245.01.11.

Beaumont, C., Jamieson, R.A., Nguyen, M.H., Lee, B., 2001. Himalayan tectonics explained by extrusion of a low-viscosity crustal channel coupled to focused surface denudation. Nature 414, 738–742. https://doi.org/10.1038/414738a.

Bellido, F., Capote, R., Casquet, C., Fúster, J.M., Navidad, M., Peinado, M., Villaseca, C., 1981. Caracteres generales del Cinturon Hercinico en el Sector Oriental del Sistema Central Español. Cuadernos Geol. Ibérica 7, 15–51.

Borg, I., Handin, J., 1966. Experimental deformation of crystalline rocks. Tectonophysics 3, 249–367.

Capote, R., Casquet, C., Fernández Casals, M.J., 1981. La tectónica hercínica de cabalgamientos en el Sistema Central Español. Cuadernos Geol. Ibérica 7, 455–469.

Capote, R., Martín González, F., Tsige, M., 2000. Tectónica extensional en el Sistema Central: La Zona de Cizalla Dúctil de Santa María de la Alameda. Geogaceta 28, 27–29.

Cardozo, N., Allmendinger, R.W., 2013. Spherical projections with OSXStereonet. Comput. Geosci. 51, 193–205.

Carreras, J., Druguet, E., 2019. Complex fold patterns developed by progressive deformation. J. Struct. Geol. 125, 195–201.

Carreras, J., Druguet, E., Griera, A., 2005. Shear zone-related folds. J. Struct. Geol. 27, 1229–1251.

Carter, N.L., Christie, J.M., Griggs, D.T., 1964. Experimental Deformation and Recrystallization of Quartz. J. Geol. 72, 687–733.

Cawood, T.K., Platt, J.P., 2021. What controls the width of ductile shear zones? Tectonophysics 816, 229033. https://doi.org/10.1016/j.tecto.2021.229033.

Dallmeyer, R.D., Martínez Catalán, J.R., Arenas, R., Gil Ibarguchi, J.I., Gutiérrez-Alonso, G., Farias, P., Bastida, F., Aller, J., 1997. Diachronous Variscan tectonothermal activity in the NW Iberian Massif: evidence from 40Ar/39Ar dating of regional fabrics. Tectonophysics 277, 307–337.

Díaz-Azpiroz, M., Fernández, C., Czeck, D.M., 2019. Are we studying deformed rocks in the right sections? Best practices in the kinematic analysis of 3D deformation zones. J. Struct. Geol. 125, 218–225.

Díez Balda, M.A., Martínez Catalán, J.R., Ayarza, P., 1995. Syn-collisional extensional collapse parallel to the orogenic trend in a domain of steep tectonics: the Salamanca detachment zone (Central Iberian Zone, Spain). J. Struct. Geol. 17, 163–182.

Díez Fernández, R., Arenas, R., 2015. The late Devonian Variscan suture of the Iberian Massif: a correlation of high-pressure belts in NW and SW Iberia. Tectonophysics 654, 96–100.

Díez Fernández, R., Pereira, M.F., 2016. Extensional orogenic collapse captured by strike-slip tectonics: constrains from structural geology and U-Pb geochronology of the Pinhel shear zone (Variscan orogen, Iberian Massif). Tectonophysics 691, 290–310.

Díez Fernández, R., Pereira, M.F., 2017. Strike-slip shear zones of the Iberian Massif: are they coeval? Lithosphere 9 (5), 726–744.

Díez Fernández, R., Martínez Catalán, J.R., Gómez Barreiro, J., Arenas, R., 2012. Extensional flow during gravitational collapse: a tool for setting plate convergence (Padrón migmatitic dome, Variscan belt, NW Iberia). J. Geol. 120, 83–103.

Díez Fernández, R., Gómez Barreiro, J., Martínez Catalán, J.R., Ayarza, P., 2013. Crustal thickening and attenuation as revealed by regional fold interference patterns: Ciudad Rodrigo basement area (Salamanca, Spain). J. Struct. Geol. 46, 115–128.

Díez Fernández, R., Arenas, R., Pereira, M.F., Sánchez-Martínez, S., Albert, R., Martín Parra, L.M., Rubio Pascual, F.J., Matas, J., 2016. Tectonic evolution of Variscan Iberia: Gondwana-Laurussia collision revisited. Earth Sci. Rev. 162, 269–292.

Díez Fernández, R., Martín Parra, L.M., Rubio Pascual, F.J., 2017. Extensional flow produces recumbent folds in syn-orogenic granitoids (Padrón migmatitic dome, NW Iberian Massif). Tectonophysics 703-704, 69–84.

Díez Fernández, R., Jiménez-Díaz, A., Arenas, R., Pereira, M.F., Fernández-Suárez, J., 2019a. Ediacaran obduction of a Fore-arc ophiolite in SW Iberia: a turning point in the evolving geodynamic setting of Peri-Gondwana. Tectonics 38, 95–119.

Díez Fernández, R., Rubio Pascual, F.J., Martín Parra, L.M., 2019b. Re-folded structure of syn-orogenic granitoids (Padrón dome, NW Iberia): assessing rheological evolution of cooling continental crust in a collisional setting. Geosci. Front. 10, 651–669.

Doblas, M., 1991. Late hercynian extensional and transcurrent tectonics in Central Iberia. Tectonophysics 191, 325–334.

Doblas, M., López-Ruiz, J., Oyarzun, R., Mahecha, V., Moya, Y.S., Hoyos, M., Cebriá, J.-M., Capote, R., Enrile, J.H., Lillo, J., Lunar, R., Ramos, A., Sopeña, A., 1994. Extensional tectonics in the Central Iberian Peninsula during the Variscan to Alpine transition. Tectonophysics 238, 95–116.

Escuder Viruete, J., Hernáiz Huerta, P.P., Valverde-Vaquero, P., Rodríguez Fernández, R., Dunning, G., 1998. Variscan syncollisional extension in the Iberian Massif: structural, metamorphic and geochronological evidence from the Somosierra sector of the Sierra de Guadarrama (Central Iberian Zone, Spain). Tectonophysics 290, 87–109.

Escuder Viruete, J.E., Arenas, R., Martínez Catalán, J.R., 1994. Tectonothermal evolution associated with Variscan crustal extension in the Tormes gneiss dome (NW Salamanca, Iberian massif, Spain). Tectonophysics 238, 117–138.

Fernández Rodríguez, C., 1990. Evolución durante el Pérmico inferior de las fallas de la región de Pálmaces de Jadraque-Angón (borde SE del Sistema Central Español). Geogaceta 9, 50–52.

Fernández Rodríguez, C., 1991. Estudio de los procesos de deformación en la zona de Cizalla de Hiendelaencina (Sistema Central español). PhD thesis. Complutense University of Madrid, p. 522.

Franke, W., Cocks, L.R.M., Torsvik, T.H., 2017. The palaeozoic variscan oceans revisited. Gondwana Res. 48, 257–284.

Froitzheim, N., 1992. Formation of recumbent folds during synorogenic crustal extension (Austroalpine nappes, Switzerland). Geology 20, 923–926.

García-Lasanta, C., Oliva-Urcia, B., Román-Berdiel, T., Casas, A.M., Gil-Peña, I., Sánchez-Moya, Y., Sopeña, A., Hirt, A.M., Mattei, M., 2015. Evidence for the Permo-Triassic transtensional rifting in the Iberian Range (NE Spain) according to magnetic fabrics results. Tectonophysics 651-652, 216–231.

García-Senz, J., Ja, R.A., Pedrera, A., 2019. The North Iberian Continental Margin. In: The Geology of Iberia: A Geodynamic Approach: Volume 3: The Alpine Cycle. Springer, pp. 1–171.

Gómez Barreiro, J., Martínez Catalán, J.R., Díez Fernández, R., Arenas, R., Díaz García, F., 2010. Upper crust reworking during gravitational collapse: the Bembibre-Pico Sacro detachment system (NW Iberia). J. Geol. Soc. 167, 769–784.

González Lodeiro, F., 1980. Estudio geológico estructural de la terminación oriental de la Sierra de Guadarrama (Sistema Central Español). PhD thesis. University of Salamanca, p. 366.

Gottschalk, R.R., Kronenberg, A.K., Russell, J.E., Handin, J., 1990. Mechanical anisotropy of gneiss: failure criterion and textural sources of directional behavior. J. Geophys. Res. 95, 21613–21634.

Gutiérrez-Alonso, G., Collins, A.S., Fernández-Suárez, J., Pastor-Galán, D., González-Clavijo, E., Jourdan, F., Weil, A.B., Johnston, S.T., 2015. Dating of lithospheric buckling: 40Ar/39Ar ages of syn-orocline strike-slip shear zones in northwestern Iberia. Tectonophysics 643, 44–54.

Harris, L.B., Koyi, H.A., Fossen, H., 2002. Mechanisms for folding of high-grade rocks in extensional tectonic settings. Earth Sci. Rev. 59, 163–210.

Heredia, N., Martín-González, F., Farias, P., García-Sansegundo, J., Pedreira, D., Gonzalo-Guerra, B., García-Davia, G., Mateos, G., Flórez-Rodríguez, A.G., 2022.

Geology of the Cabuérniga Fault System: evolution of a large Alpine structure with Variscan inheritance. J. Maps 1-10. https://doi.org/10.1080/17445647.2021.2010612.
Hernaiz Huerta, P.P., Escuder Viruete, J.E., Rodríguez Fernández, L.R., Valverde Vaquero, P., Dunning, G., 1996. Evolución estructural de la zona de cizalla extensional de Berzosa-Riaza, sector de Somosierra, Sistema Central Español. Geogaceta 20, 875–878.
Holdsworth, R.E., Butler, C.A., Roberts, A.M., 1997. The recognition of reactivation during continental deformation. J. Geol. Soc. 154, 73–78.
Holdsworth, R.E., Handa, M., Miller, J.A., Buick, I.S., 2001. Continental reactivation and reworking: an introduction. In: Miller, J.A., Holdsworth, R.E., Buick, I.S., Hand, M. (Eds.), Continental Reactivation and Reworking, 184(1). Geological Society, London, Special Publications, pp. 1–12.
Jamieson, R.A., Beaumont, C., Nguyen, M.H., Culshaw, N.G., 2007. Synconvergent ductile flow in variable-strength continental crust: Numerical models with application to the western Grenville orogen. Tectonics 26, TC5005.
Kley, J., Voigt, T., 2008. Late cretaceous intraplate thrusting in Central Europe: effect of Africa-Iberia-Europe convergence, not Alpine collision. Geology 36 (11), 839–842.
Lago, M., Arranz, E., Pocoví, A., Galé, C., Gil-Imaz, A., 2004. Lower Permian magmatism of the Iberian Chain, Central Spain, and its relationship to extensional tectonics. Permo-Carboniferous Magmatism and Rifting in Europe. Geol. Soc. Lond., Spec. Publ. 223, 465–490.
Linnemann, U., Gerdes, A., Hofmann, M., Marko, L., 2014. The Cadomian Orogen: neoproterozoic to Early Cambrian crustal growth and orogenic zoning along the periphery of the West African Craton—Constraints from U–Pb zircon ages and Hf isotopes (Schwarzburg Antiform, Germany). Precambrian Res. 244, 236–278. https://doi.org/10.1016/j.precamres.2013.08.007.
Lloret, J., López-Gómez, J., Heredia, N., Martín-González, F., de la Horra, R., Borruel-Abadía, V., Ronchi, A., Barrenechea, J.F., García-Sansegundo, J., Galé, C., Ubide, T., Gretter, N., Diez, J.B., Juncal, M., Lago, M., 2021. Transition between Variscan and Alpine cycles in the Pyrenean-Cantabrian Mountains (N Spain): Geodynamic evolution of near-equator European Permian basins. Glob. Planet. Chang. 103677.
López-Gómez, J., Arche, A., Pérez-López, A., 2002. Permian and Triassic. In: Gibbons, W., Moreno, T. (Eds.), The Geology of Spain. Geological Society of London, pp. 185–212.
Macaya, J., González-Lodeiro, F., Martínez-Catalán, J.R., Álvarez, F., 1991. Continuous deformation, ductile thrusting and backfolding of cover and basement in the Sierra de Guadarrama, Hercynian orogen of Central Spain. Tectonophysics 191, 291–309.
Macchiavelli, C., Vergés, J., Schettino, A., Fernàndez, M., Turco, E., Casciello, E., Torne, M., Pierantoni, P.P., Tunini, L., 2017. A New Southern North Atlantic Isochron Map: insights into the drift of the Iberian Plate since the late cretaceous. J. Geophys. Res. Solid Earth 122 (12), 9603–9626.
Martínez Catalán, J.R., 2011. Are the oroclines of the Variscan belt related to late Variscan strike-slip tectonics? Terra Nova 23, 241–247.
Martínez Catalán, J.R., González Lodeiro, F., González Clavijo, E., Fernández, C., Díez Montes, A., 2004. Zona Centroibérica: Dominio del Ollo de Sapo, Estructura. In: Vera, J.A. (Ed.), Geología de España. SGE-IGME, Madrid, pp. 75–78.
Martínez Catalán, J.R., Arenas, R., Díaz García, F., Gómez Barreiro, J., González Cuadra, P., Abati, J., Castiñeiras, P., Fernández-Suárez, J., Sánchez Martínez, S., Andonaegui, P., González Clavijo, E., Díez Montes, A., Rubio Pascual, F.J., Valle Aguado, B., 2007. Space and time in the tectonic evolution of the northwestern Iberian Massif. Implications for the Variscan belt. In: Hatcher, R.D., Carlson, M.P., McBride, J.H., y and Martínez Catalán, J.R. (Eds.), 4-D Framework of Continental Crust. Geological Society of America Memoir, Boulder, Colorado, pp. 403–423.
Martínez Catalán, J.R., Rubio Pascual, F.J., Díez Montes, A., Díez Fernández, R., Gómez Barreiro, J., Dias da Silva, Í., González Clavijo, E., Ayarza, P., Alcock, J.E., 2014. The late Variscan HT/LP metamorphic event in NW and Central Iberia: relationships to crustal thickening, extension, orocline development and crustal evolution. In: Schulmann, K., Martínez Catalán, J.R., Lardeaux, J.M., Janoušek, V., Oggiano, G. (Eds.), The Variscan Orogeny: Extent, Timescale and the Formation of the European Crust, 405(1). Geological Society of London Special Publication, pp. 225–247.
Martínez Catalán, J.R., Schulmann, K., Ghienne, J.F., 2021. The Mid-Variscan Allochthon: Keys from correlation, partial retrodeformation and plate-tectonic reconstruction to unlock the geometry of a non-cylindrical belt. Earth Sci. Rev. 220, 1–65.
Martín-González, F., Heredia, N., 2011a. Geometry, structures and evolution of the western termination of the Alpine-Pyrenean Orogen reliefs (NW Iberian Peninsula). J. Iber. Geol. 37 (2), 103–120.
Martín-González, F., Heredia, N., 2011b. Complex tectonic and tectonostratigraphic evolution of an Alpine foreland basin: the western Duero Basin and the related Tertiary depressions of the NW Iberian Peninsula. Tectonophysics 502 (1–2), 75–89.
Matte, P., 2001. The Variscan collage and orogeny (480-290 Ma) and the tectonic definition of the Armorica microplate: a review. Terra Nova 13, 122–128.
Means, W.D., Hobbs, B.E., Lister, G.S., Williams, P.F., 1980. Vorticity and non-coaxiality in progressive deformations. J. Struct. Geol. 2, 371–378.
Merle, O., 1998. Emplacement mechanisms of nappes and thrust sheets. Springer, Dordrecht, Netherlands, p. 160.
Michael, A.J., 1984. Determination of stress from slip data: faults and folds. J. Geophys. Res. Abstr. 89, 11517–11526.
Moreno-Martín, D., Díez Fernández, R., de Vicente, G., Fernández, C., Gomez Barreiro, J., 2021. Structural data from Hiendelaencina shear zone (Guadalajara, Spain). Mendeley Data V1. https://doi.org/10.17632/bn9hbvr336.1.
Nocquet, J.-M., 2012. Present-day kinematics of the Mediterranean: a comprehensive overview of GPS results. Tectonophysics 579, 220–242.
Pastor-Galán, D., 2022. From supercontinent to superplate: late Paleozoic Pangea's inner deformation suggests it was a short-lived superplate. Earth Sci. Rev. 226, 103918.
Platt, J.P., Behr, W.M., Johanesen, K., Williams, J.R., 2013. The Betic-Rif Arc and its Orogenic Hinterland: a review. Annu. Rev. Earth Planet. Sci. 41, 313–357.
Querol, R., 1989. Geología del subsuelo de la Cuenca del Tajo. ITGE-ETSI de Minas, Madrid, Spain, pp. 1–48.
Ramsay, J.G., 1967. Folding and Fracturing of Rocks. McGraw-Hill, New York, USA, p. 568.
Rat, J., Mouthereau, F., Brichau, S., Crémades, A., Bernet, M., Balvay, M., Ganne, J., Lahfid, A., Gautheron, C., 2019. Tectonothermal Evolution of the Cameros Basin: Implications for Tectonics of North Iberia. Tectonics 38 (2), 440–469.
Ribeiro, A., Munhá, J., Dias, R., Mateus, A., Pereira, E., Ribeiro, L., Fonseca, P., Araújo, A., Oliveira, T., Romão, J., Chaminé, H., Coke, C., Pedro, J., 2007. Geodynamic evolution of the SW Europe Variscides. Tectonics 26, 1–24.
Rubio Pascual, F.J., 2013. Evolución tectonotermal varisca del Sistema Central en Somosierra-Honrubia. PhD thesis. Complutense University of Madrid, p. 360.
Rubio Pascual, F.J., Arenas, R., Martínez Catalán, J.R., Fernández, L.R.R., Wijbrans, J.R., 2013. Thickening and exhumation of the Variscan roots in the Iberian Central System: tectonothermal processes and 40Ar/39Ar ages. Tectonophysics 587, 207–221.
Rubio Pascual, F.J., López-Carmona, A., Arenas, R., 2016. Thickening vs. extension in the Variscan belt: P–T modelling in the Central Iberian autochthon. Tectonophysics 681, 144–158.
Schröeder, E., 1930. La zona limítrofe del Guadarrama y las Cadenas Hespéricas. Publicaciones Extranjeras Geología de España 4, 294–325.
Shea, W.T., Kronenberg, A.K., 1992. Rheology and deformation mechanisms of an isotropic mica schist. J. Geophys. Res. 97, 15201–15237.
Shea, W.T., Kronenberg, A.K., 1993. Strength and anisotropy of foliated rocks with varied mica contents. J. Struct. Geol. 15, 1097–1121.
Simancas, J.F., Ayarza, P., Azor, A., Carbonell, R., Martínez Poyatos, D., Pérez-Estaún, A., González Lodeiro, F., 2013. A seismic geotraverse across the Iberian Variscides: Orogenic shortening, collisional magmatism, and orocline development. Tectonics 32, 417–432.
Soers, E., 1972. Stratigraphie et geologie structurale de la partie orientale de la Sierra de Guadarrama (Espagne Centrale). Stud. Geol. 4, 7–94.
Sopeña, A., 1979. Estratigrafía del Pérmico y Triásico del noroeste de la provincia de Guadalajara. PhD thesis. Complutense University of Madrid, p. 329.
Sopeña, A., López, J., Arche, A., Pérez-Arlucea, M., Ramos, A., Virgili, C., Hernando, S., 1988. Permian and Triassic Rift Basins of the Iberian Peninsula. In: Manspeizer, W. (Ed.), Triassic-Jurassic Rifting. Continental breakup and the Origin of the Atlantic Ocean and passive margins. Devel. Geotectonics, 22 (B). Elsevier, Amsterdam, pp. 757–782.
Valverde Vaquero, P., Dunning, G., Hernaiz Huerta, P.P., Escuder Viruete, J., Rodríguez Fernández, R., 1996. La extensión Sin~ Colisional en la Zona Centro Ibérica: restricciones temporales impuestas por edades U-Pb en monacitas del sector de Somosierra, Sistema Central Español. Geogaceta 20 (4), 883–886.
Vavryčuk, V., 2014. Iterative joint inversion for stress and fault orientations from focal mechanisms. Geophys. J. Int. 199, 69–77.
Vergés, J., Fernández, M., Martínez, A., 2002. The Pyrenean orogen: pre-, syn-, and post-collisional evolution. In: Rosenbaum, G., Lister, G. (Eds.), Reconstruction of the Evolution of the Alpine-Himalayan Orogen. Journal of the Virtual Explorer, Electronic Edition, 8 (4). https://doi.org/10.3809/jvirtex.2002.00058.
de Vicente, G., Vegas, R., Muñoz-Martín, A., Silva, P.G., Andriessen, P., Cloetingh, S., González-Casado, J.M., Van Wees, J.D., Álvarez, J., Carbó, A., Olaiz, A., 2007. Cenozoic thick-skinned and topography evolution of the Spanish central system. Glob. Planet. Chang. 58, 335–381.
de Vicente, G., Vegas, R., Muñoz-Martín, A., Van Wees, J.D., Casas-Sáinz, A., Sopeña, A., Sánchez-Moya, Y., Arche, A., López-Gómez, J., Olaiz, A., Fernández-Lozano, J., 2009. Oblique strain partitioning and transpression on an inverted rift: the Castilian Branch of the Iberian Chain. Tectonophysics 470, 224–242.
de Vicente, G., Cunha, P.P., Muñoz-Martín, A., Cloetingh, S.A.P.L., Olaiz, A., Vegas, R., 2018. The Spanish-Portuguese Central System: an example of intense Intraplate Deformation and Strain Partitioning. Tectonics 37, 4444–4469.
de Vicente, G., Muñoz-Martín, A., Díez Fernández, R., Olaiz, A., 2021. Kink bands alpinos en rocas foliadas del basamento varisco del Sistema Central. Geogaceta 69, 7–10.
de Vicente, G., Díez Fernández, R., Olaiz, A., Muñoz-Martín, A., 2022. Variscan inheritance induces Alpine upper crustal delamination in East Spanish–Portuguese Central System. Tectonics 41. https://doi.org/10.1029/2022TC007315.
Warren, J.M., Hirth, G., 2006. Grain size sensitive deformation mechanisms in naturally deformed peridotites. Earth Planet. Sci. Lett. 248 (1), 438–450. https://doi.org/10.1016/j.epsl.2006.06.006.